hydrogen

MDPI

Review

Contribution of Severe Plastic Deformation via High-Pressure Torsion to the Hydrogen Cycle: From Hydrogen Production and Storage to Hydrogen Embrittlement

Kaveh Edalati

WPI, International Institute for Carbon Neutral Energy Research (WPI-I2CNER), Kyushu University, Fukuoka 819-0395, Japan; kaveh.edalati@kyudai.jp; Tel.: +81-92-802-6744

Abstract

Hydrogen is a key energy carrier for achieving carbon neutrality, yet its widespread deployment is hindered by challenges associated with efficient hydrogen production, safe and reversible hydrogen storage, and hydrogen-induced embrittlement. Severe plastic deformation processes, particularly high-pressure torsion (HPT), have emerged as a powerful approach capable of addressing these challenges through extreme grain refinement, defect engineering, phase stabilization far from equilibrium, and synthesis of novel materials. This article reviews the impact of HPT on hydrogen-related materials, covering hydrogen production, hydrogen storage, and hydrogen embrittlement resistance. For hydrogen production, HPT enables the synthesis of nanostructured, defect-rich, and compositionally complex compounds, including high-entropy oxides and oxynitrides, which exhibit enhanced hydrolytic, electrocatalytic, photocatalytic, photoelectrocatalytic, and photoreforming performance. For hydrogen storage, HPT fundamentally modifies hydrogenation activation and kinetics, and modifies thermodynamics by hydrogen binding energy engineering, enabling reversible hydrogen storage at room temperature in systems such as Mg-based and high-entropy alloys. For hydrogen embrittlement resistance, HPT under optimized conditions suppresses hydrogen-assisted fracture by engineering ultrafine grains and defects (vacancies, dislocations, Lomer–Cottrell locks, D-Frank partial dislocations, stacking faults, twins, and grain boundaries) that control hydrogen diffusion, trapping, and strain localization. By integrating insights across these three domains, this article highlights HPT as a transformative strategy for developing next-generation hydrogen materials and identifies key opportunities for future research at the intersection of severe plastic deformation and hydrogen technologies.

Keywords: severe plastic deformation (SPD); hydrogen storage materials; photocatalysis; electrolysis; hydrolysis; hydrogen compatibility

Check for updates

Academic Editors: Samuel Simon Araya and Vincenzo Liso

Received: 3 January 2026
Revised: 18 January 2026
Accepted: 28 January 2026
Published: 4 February 2026

Copyright: © 2026 by the author. Licensee MDPI, Basel, Switzerland. This article is an open access article distributed under the terms and conditions of the Creative Commons Attribution (CC BY) license.

1. Introduction

Hydrogen is widely recognized as a key energy carrier for achieving carbon neutrality due to its high gravimetric energy density, clean combustion products, and compatibility with diverse energy conversion technologies [1–3]. Hydrogen can be produced from a wide range of resources, including water, biomass, hydrocarbons, and industrial waste streams, and can be utilized in fuel cells, internal combustion engines, chemical synthesis, and metallurgical processes [1–3]. As a result, hydrogen has attracted sustained interest in the energy, materials science, and engineering communities. However, despite decades

of research and development, the large-scale implementation of hydrogen technologies remains limited by several fundamental challenges related to hydrogen production [4,5], storage [6,7], utilization [8,9], and material degradation/embrittlement [10,11].

Hydrogen production is still dominated by fossil-fuel-based processes, while low-carbon routes such as water electrolysis, photocatalytic water splitting, and hydrolytic reactions require significant improvements in efficiency, durability, and cost-effectiveness [12,13]. In many cases, the bottlenecks are not solely associated with reaction thermodynamics, but rather with sluggish kinetics, insufficient active sites, poor charge transport, and limited long-term stability of the materials involved [12,13]. These issues are particularly severe for non-noble-metal-based catalysts and photocatalysts, which are essential for scalable and sustainable hydrogen production [14,15].

Hydrogen storage represents another major barrier to the hydrogen economy. Although hydrogen has an exceptionally high gravimetric energy density, its low volumetric density makes storage challenging [16,17]. Physical storage methods, such as compressed or liquefied hydrogen, require high pressures or cryogenic temperatures and raise safety and efficiency concerns [16,17]. Solid-state hydrogen storage using metals, alloys, and complex hydrides offers a promising alternative, but practical implementation is hindered by slow hydrogen absorption and desorption kinetics, unfavorable thermodynamics, poor reversibility, and degradation during cycling [6,7]. Achieving fast, reversible hydrogen storage at near-ambient conditions remains one of the most demanding challenges in hydrogen materials research [18].

In parallel, hydrogen embrittlement poses a serious reliability and safety issue for structural materials used in hydrogen production, transportation, and storage systems [19,20]. Hydrogen can severely degrade mechanical properties by interacting with lattice defects, grain boundaries, dislocations, and phase interfaces, leading to premature failure even at low hydrogen concentrations [19,20]. While extensive efforts have been devoted to understanding hydrogen embrittlement mechanisms, effective strategies to design materials with high strength and intrinsic resistance to hydrogen-induced degradation are still limited [10,11].

A common feature underlying hydrogen production, storage, and embrittlement is the critical role of lattice defects, microstructure, and metastable phases [4–11]. Conventional approaches to improve hydrogen-related properties typically rely on alloying, compositional tuning, surface coatings, or chemical routes [12–20]. While these methods have achieved some success in controlling crystal structure, microstructure, and lattice defects, they often introduce compositional complexity, limited tunability of defect structures, or sometimes poor stability. In this context, severe plastic deformation (SPD) has emerged as a powerful physical approach for tailoring microstructure and defect states without changing their chemical composition [21,22]. Among various SPD techniques, high-pressure torsion (HPT) is particularly unique to the hydrogen field because it enables the introduction of extremely high shear strains and nanostructural features in almost any kind of material [23,24]. Moreover, it allows the synthesis of new materials for different functional applications [25,26].

This article, after an introduction about HPT, provides an overview of the impact of HPT on hydrogen-related materials, with a focus on the author's contributions. Emphasis is placed on a mechanistic understanding of how HPT-induced microstructures and defects or synthesis influence hydrogen production, storage, and embrittlement behavior. A flowchart illustrating the contents of the manuscript, materials, and their applications is shown in Figure 1.

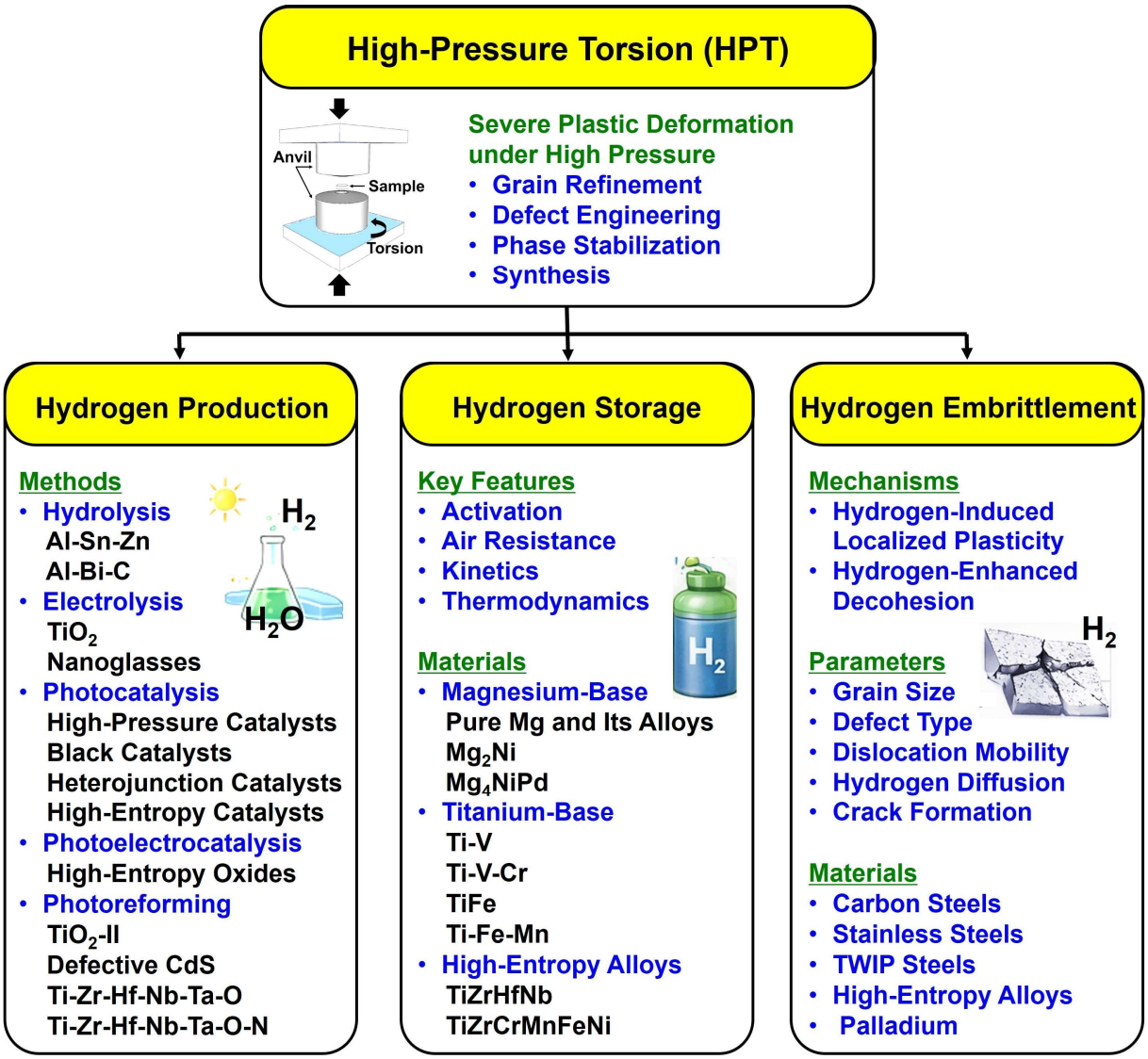


Figure 1. Flowchart of this article illustrating the contents, HPT effects, materials, and reported applications for hydrogen production, hydrogen storage, and hydrogen embrittlement resistance.

2. High-Pressure Torsion

The HPT process is a classic technique in which a sample is subjected to concurrent high compressive pressure and torsional shear strain [27]. In a typical HPT process, a disc-shaped sample with a thickness of several hundred micrometers is placed between two anvils and compressed under pressures in the range of several gigapascals while one anvil is rotated relative to the other [23,24]. In addition to typical HPT using disc samples, there are modifications of the method for processing of rings [28] as well as continuous processing of wires and strips [29], as shown in Figure 2. Unlike conventional plastic deformation methods, HPT is performed under quasi-hydrostatic pressure, which suppresses crack formation and enables deformation of a wide range of materials, including metals [30,31], intermetallics [32,33], ceramics [34,35], and composite systems [36,37].

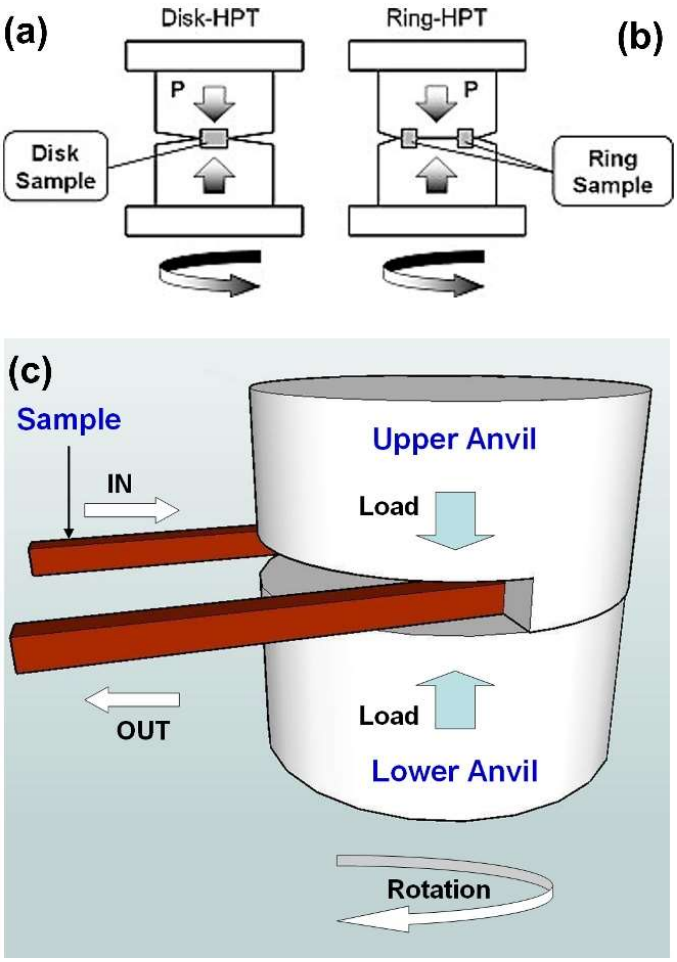


Figure 2. Schematics of (**a**) HPT using a disk [28], (**b**) HPT using a ring [28], and (**c**) continuous HPT using a strip [29].

One of the most significant features of HPT is its ability to generate extremely small grains (usually at submicrometer or nanometer scales) and a large fraction of high-angle grain boundaries (Figure 3a [38]). Moreover, a high density of lattice defects is formed in hydrogen-related materials, such as twins (Figure 3b [39]), stacking faults (Figure 3c [40]), and dislocations, including Lomer–Cottrell dislocation locks (Figure 3d [41]) and D-Frank partial dislocations (Figure 3e [41]). Vacancies were also frequently reported in HPT-processed metals [42,43], while other kinds of vacancies were reported in ceramics, including oxygen vacancies (Figure 3f [44]) and sulfur vacancies (Figure 3g [45]). Despite the linear dependence of imposed shear strain on radial distance from the rotation center in HPT [23,24], under sufficiently high strains, microstructural saturation is commonly achieved, resulting in the appearance of homogeneous ultrafine-grained or nanocrystalline structures from the disk center to the periphery [46,47]. In addition, HPT can induce phase transformations [48,49] and promote solid-state reactions for the synthesis of new materials [50,51] that are otherwise difficult to achieve. A few examples of such structural changes are shown in Figure 4a for partial amorphization in a Ti-Fe-Mn intermetallic [52], Figure 4b for high-pressure γ phase formation in MgH_2 [53], Figure 4c for high-pressure rocksalt phase formation in ZnO [54], Figure 4d for TiFe synthesis by HPT [55], and Figure 4e for Mg_4NiP synthesis by HPT [56].

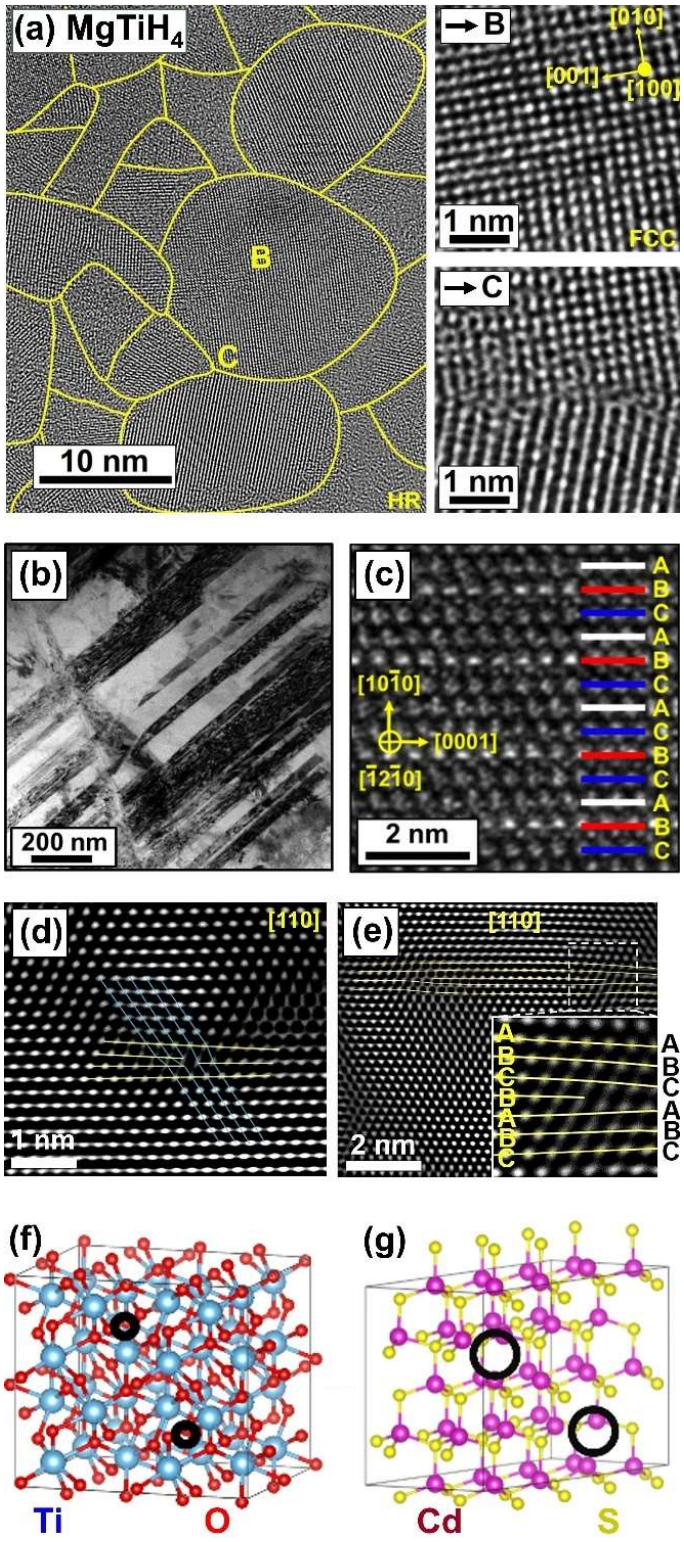


Figure 3. Formation of crystal lattice defects by HPT processing. (**a**) Grain boundaries in $MgTiH_4$ hydride [38], (**b**) twins in TWIP steel [39], (**c**) stacking faults in $MgNi_2$ intermetallic [40], (**d**) Lomer–Cottrell dislocation locks in CrMnFeCoNi high-entropy alloy [41], (**e**) D-Frank partial dislocations in CrMnFeCoNi high-entropy alloy [41], and (**f**) simulated oxygen vacancies in TiO_2 [44] and (**g**) simulated sulfur vacancies in CdS [45].

Compared with other SPD techniques such as equal-channel angular pressing [57,58], accumulative roll bonding [59,60], and multidirectional forging [61,62], HPT has been more widely applied to hydrogen-related materials due to its high strain and applicability to

various kinds of metallic and non-metallic materials [63,64]. Although HPT was historically developed as a laboratory-scale technique for fundamental studies of plastic deformation under high pressure [25], extensive work has been conducted to synthesize various materials by applying ultra-severe plastic deformation via HPT (i.e., applying shear strains over 1000) [65]. The capability of HPT in defect engineering and material synthesis has led to significant contributions of the method to the hydrogen field, as reviewed in this article.

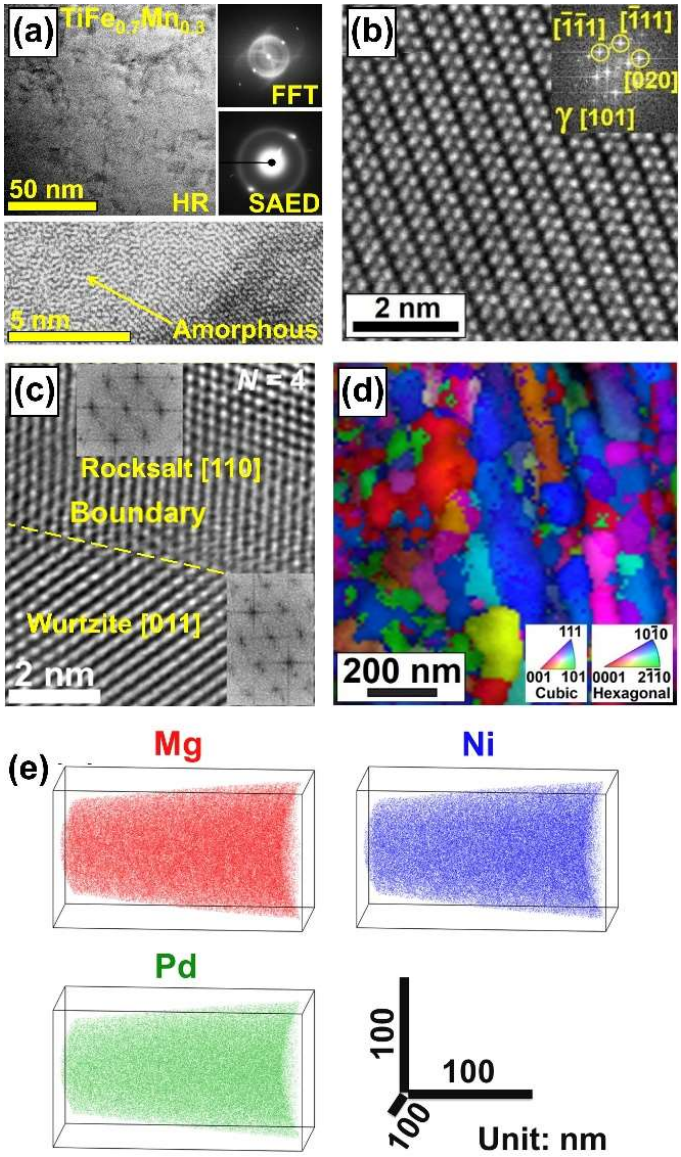


Figure 4. Formation of metastable phases and solid-state reactions by HPT processing. (**a**) Amorphous phase in $TiFe_{0.7}Mn_{0.3}$ intermetallic [52], (**b**) high-pressure γ phase in MgH_2 hydride [53], (**c**) high-pressure rocksalt phase in ZnO oxide [54], (**d**) mechanically alloyed TiFe intermetallic [55], and (**e**) mechanically alloyed Mg_4NiPd alloy [56].

3. Implication of High-Pressure Torsion for Hydrogen Production

Hydrogen production methods are broadly categorized by their environmental impact and energy sources, with blue and green hydrogen representing two key pathways. Blue hydrogen is produced from natural gas through a conventional process called steam methane reforming, which generates hydrogen but also CO_2 [66,67]. The blue designation comes from the subsequent capture and storage of most of this CO_2, reducing its atmospheric release compared to conventional steam reforming [66,67]. In contrast,

green hydrogen is produced using entirely renewable energy, resulting in zero carbon emissions [68,69]. The most established method for green hydrogen is electrolysis, where an electric current splits water into hydrogen and oxygen, while the electricity is sourced from renewables like wind or solar, making the process more environmentally friendly compared to conventional electrolysis [68,69]. Beyond electrolysis, several methods aim to produce green hydrogen more directly from sunlight and water. Photocatalysis uses semiconductor materials to absorb sunlight and directly catalyze water splitting in a single step [70,71]. Photoelectrocatalysis combines principles of photocatalysis and electrolysis, using a light-absorbing electrode in an electrochemical cell to drive the water-splitting reaction with solar energy, often achieving higher efficiencies than photocatalysis alone [72,73]. Another solar-driven process, photoreforming, typically uses sunlight and a catalyst to generate hydrogen from water and waste compounds such as plastic waste [74,75]. It is crucial to distinguish these processes from hydrolysis, a term for any reaction of water in which hydrogen is produced [76,77]. In this section, the publications on the use of HPT for hydrogen production, which are still limited to the current author and his colleagues, are reviewed.

3.1. Hydrolytic Hydrogen Production

Hydrolytic hydrogen production from the reaction of water with aluminum or its alloys has been of scientific interest because aluminum forms a passive oxide layer on the surface, which hinders the reaction [78–80]. The HPT processing is effective for overcoming the native passivation of aluminum in neutral water [81]. The intimate mixing of aluminum with elements of more positive electrode potential, such as tin or bismuth, by HPT, creates a high density of internal nano-galvanic cells. In these cells, the aluminum matrix acts as a sacrificial anode, significantly accelerating its corrosion (oxidation) by water, while hydrogen is evolved at the cathodic sites. The research demonstrates that increasing the number of HPT turns (i.e., shear strain) directly improves microstructural homogeneity and the distribution of these galvanic couples, leading to higher hydrogen generation rates and yields [81–83].

Beyond forming nano-galvanic cells, HPT processing enables the strategic design of multi-component systems that control synergistic mechanisms for unprecedented performance. The work on Al-Sn-Zn alloys shows that the addition of zinc, homogeneously distributed via HPT, promotes severe pitting corrosion, initiating localized attack that further accelerates the hydrolysis reaction [83]. As shown in Figure 5a, while as-cast and cold-rolled Al-Sn-Zn are inert to water, HPT-processed samples produce hydrogen [83]. The Al-Bi-C system exemplifies an optimized approach, combining three strategies facilitated by HPT: (1) bismuth, with a higher electrode potential than tin, creates stronger galvanic coupling with aluminum; (2) bismuth also actively shifts the pitting potential to enhance corrosive attack; and (3) the incorporation of brittle graphite particles promotes easy fragmentation of the composite during reaction, constantly exposing fresh active surface areas, leading to an increase in hydrogen production with increasing the graphite fraction, as shown in Figure 5b [82]. This multifaceted engineering resulted in achieving a remarkable hydrogen generation rate of 270 mL min^{-1} g^{-1} and a 100% theoretical yield in less than 10 min at 333 K, establishing HPT as a transformative tool for activating materials for efficient chemical hydrogen generation [82].

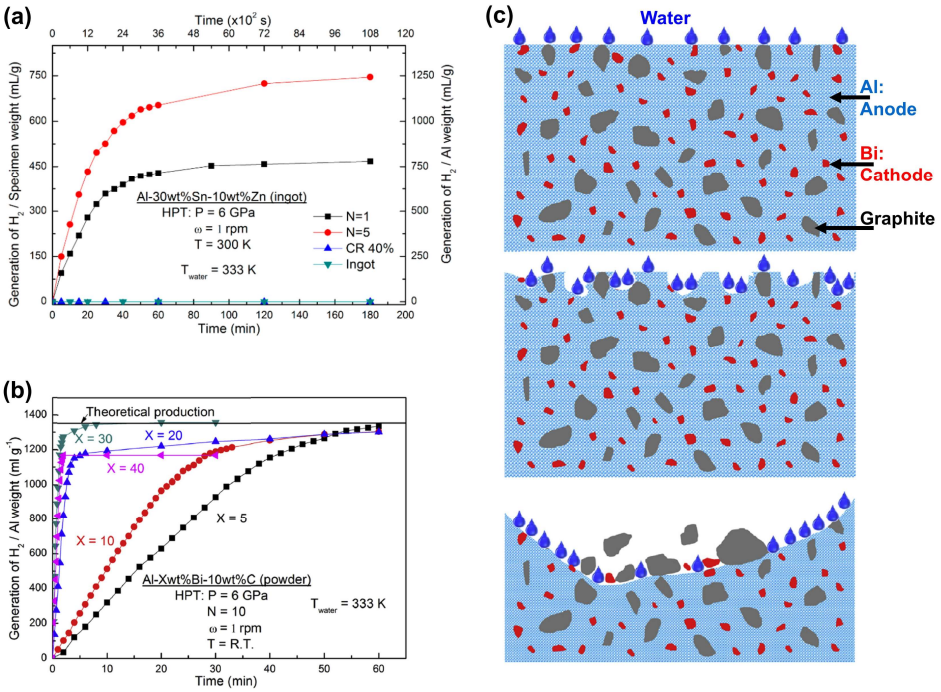


Figure 5. Enhanced hydrolytic hydrogen production by HPT processing. (**a**) Hydrogen production versus time for Al-30Sn-10Zn (wt%) processed by HPT for 1 and 5 turns compared to samples processed by ingot casting and cold rolling [83], (**b**) hydrogen production versus time for Al-XBi-10C (wt%) processed by HPT for 10 turns [82], and (**c**) schematic illustration of formation of nano-galvanic cells by HPT in Al-Bi-C and the mechanism of hydrolysis [82].

It should be noted that corrosion is not uniform in the hydrolysis of HPT-processed alloys, but is characterized by localized galvanic attack and pitting [81]. These mechanisms actively disrupt the formation of uniform oxide/corrosion products, continuously exposing fresh aluminum surfaces to sustain the reaction [83]. In systems such as Al-Bi-C, while aluminum acts as anode and Bi as cathode, the incorporation of brittle graphite particles is a strategic design choice to promote mechanical fragmentation of the composite during reaction, thereby physically breaking up any passivating layers (Figure 5c) [82].

3.2. Electrocatalytic Hydrogen Production

Electrocatalysis using electricity from renewable energies is currently the most feasible pathway to produce green hydrogen [84,85]. While HPT is highly effective for activating materials for chemical hydrolysis, its profound impact extends to the electrocatalytic hydrogen evolution reaction. The first attempt on this issue reported that the electrocatalytic hydrogen production improves with HPT processing of TiO_2 [86]. Later studies demonstrate that HPT serves as a powerful post-processing technique to transform conventional melt-spun metallic glasses into superior, noble-metal-free electrocatalysts [87–90]. For instance, subjecting a glass of $Pd_{40}Cu_{30}Ni_{10}P_{20}$ to HPT significantly increased its energy state by ~21.7 J/g by creating a high density of flow units (i.e., loosely packed, high-energy atomic regions within the amorphous matrix) and partial recrystallization [88]. This structural rejuvenation dramatically enhanced hydrogen evolution reaction performance in both acidic and alkaline media, reducing the overpotential at 10 mA cm^{-2} from 179 mV to 76 mV in 0.5 M H_2SO_4 and from 379 mV to 209 mV in 1.0 M KOH. As shown in Figure 6a, the sample processed with 5 and 10 HPT turns exhibited the lowest overpotential, highest electrochemical surface area, and best stability, outperforming the initial sample and samples processed with 1 and 2 turns. The enhanced activity is primarily attributed to these flow units, which provide more catalytically active sites and facilitate hydrogen adsorption and desorption [88].

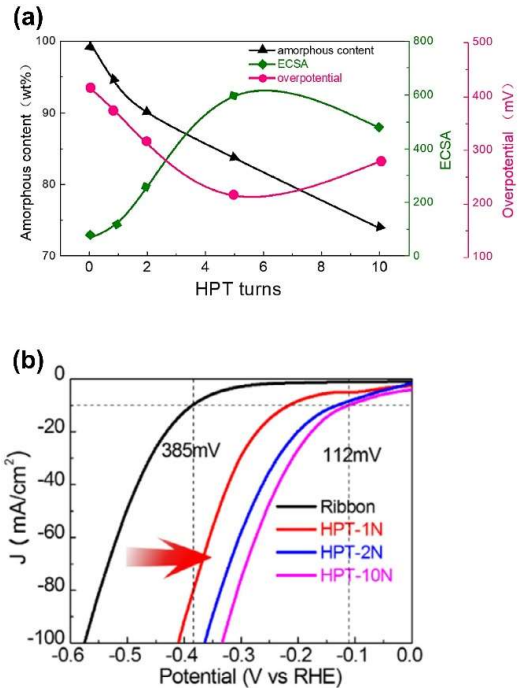


Figure 6. Enhanced electrocatalytic hydrogen production by HPT processing. (**a**) Variations in amorphous phase fraction, electrochemical surface area (ECSA), and overpotential versus number of HPT turns for $Fe_{73.5}Si_{13.5}B_9Cu_1Nb_3$ metallic glass [88], and (**b**) linear sweep voltammetry curves (current density against potential) for $Fe_{78}Si_9B_{13}$ amorphous alloy processed by HPT for 1, 2, and 10 turns compared with the initial ribbon [87].

For a Fe-based system, HPT induces a more complex microstructural evolution, creating a unique nanoglass architecture [87]. Processing amorphous $Fe_{78}Si_9B_{13}$ ribbons via HPT generates a composite structure where nanocrystallites of α-Fe, Fe_2B, and Fe_3Si (typically 5–10 nm in size) are embedded within a dominant amorphous matrix. Crucially, this process introduces a high density of interfacial regions both between these nanocrystals and the glassy matrix and within the amorphous phase itself. This nanoglass structure exhibits exceptional catalytic properties, particularly with increasing HPT turns, achieving an overpotential of just 112 mV at 10 mA cm^{-2} in 1 M KOH (Figure 6b), far superior to the as-spun amorphous ribbon (385 mV) and its fully crystalline counterpart (465 mV) [87]. Similar results on the enhancement of hydrogen production were reported for the $Fe_{75}B_{25}$ metallic glass [90]. HPT-processed $Fe_{75}B_{25}$ demonstrates remarkable long-term stability, maintaining stable performance for over 300 h and even at industrial-level current densities up to 300 mA cm^{-2}. This stability stems from the formation of a beneficial, loose layer of corrosion products (e.g., FeOOH) on the heterogeneous surface, which continues to facilitate the reaction without passivating the catalyst [90]. The performance is further improved to 81 mV after 1000 catalytic cycles, rivaling some Pd-based catalysts [89]. The interconnected interfaces and defects in the nanoglass provide a vastly increased electrochemical surface area and act as highly active sites for the water-splitting reaction [87,89]. Further results on the effect of HPT on electrolysis can be found in a recent publication [91].

3.3. Photocatalytic Hydrogen Production

The production of hydrogen via photocatalytic water splitting represents a cornerstone of solar-to-fuel conversion, offering a direct pathway to store solar energy in chemical form [92,93]. This process relies on semiconductors that absorb photons to generate electron-hole pairs, which then drive the reduction of water to hydrogen at the catalyst surface [94,95]. HPT has emerged as a transformative and versatile synthesis route in photocatalysis, extend-

ing far beyond its origins in high-pressure studies and metallic systems, as highlighted in a few review papers [96,97]. By applying intense shear strain under high pressure, HPT enables unique structural and electronic engineering of semiconductor materials that are difficult or impossible to achieve with conventional methods [98]. The application of the technique to photocatalysts can stabilize metastable structures such as high-pressure phases [54,99], generate dense defects such as vacancies to generate black catalysts [100,101], create complex composites with heterojunctions [102,103], and facilitate the synthesis of novel high-entropy compounds [104,105]. These modifications collectively tailor optical absorption, charge carrier separation, and surface reactivity (three important factors in photocatalysis [106]), positioning HPT as a powerful tool for designing advanced photocatalysts for solar fuel generation, including hydrogen production and methanation [107]. Each group of photocatalysts developed by HPT is briefly reviewed in this section.

3.3.1. High-Pressure Photocatalysts

High-pressure photocatalysts developed via HPT represent a novel and effective approach to stabilizing metastable polymorphs with tailored optical and catalytic properties. In the case of TiO_2, the high-pressure columbite or TiO_2-II phase (orthorhombic Pbcn), which is unstable under ambient conditions [108], can be successfully retained at atmospheric pressure after HPT processing of anatase (tetragonal $I4_1/amd$), as shown in Figure 7a. This phase transformation leads to enhanced hydrogen production under visible light [99] or UV light, as shown in Figure 7b [44]. Similarly, for ZnO, HPT induces the formation of a high-pressure phase, known as the rocksalt phase (cubic $Fm\bar{3}m$), as shown in the phase diagram of Figure 7c [109], alongside abundant oxygen vacancies [54]. These changes markedly improve photocatalytic hydrogen evolution with increasing HPT turns, as shown in Figure 7d [54]. These improvements are attributed not only to bandgap engineering but also to the creation of heterojunctions, increased surface-active sites, and optimized charge carrier dynamics. Density functional theory calculations further reveal that oxygen vacancies in high-pressure phases more effectively enhance light absorption and lower surface activation energies for water splitting [44]. Thus, HPT enables a dopant-free strategy to design high-performance photocatalysts by simultaneously stabilizing high-pressure polymorphs and tuning their electronic structure through defects.

3.3.2. Vacancy-Rich and Black Photocatalysts

The capability of the HPT method to introduce a large fraction of vacancies [110] has proven to be a powerful mechanical approach for synthesizing black oxide photocatalysts [35]. Such oxides are of interest due to their modified electronic structure, high light absorption, and good catalytic activity [111,112]. A prime example is the transformation of white ZrO_2, with a bandgap exceeding 5 eV, into black ZrO_2 through HPT processing [100]. HPT processing induces a stress-induced tetragonal-to-monoclinic ($P4_2/nmc$ to $P2_1/c$) phase transformation and, more critically, creates a high density of oxygen vacancies. This defect engineering leads to a dramatic bandgap reduction to around 4.0–4.3 eV, introduces sub-bandgap defect states, and significantly enhances light absorption, resulting in high photocatalytic hydrogen evolution. Other attempts to produce vacancy-rich oxides include brookite TiO_2 [113], tantalate perovskites [114], and Bi_2O_3 [101]. As shown in Figure 7e for Bi_2O_3, the formation of black oxide enhances light absorbance, thereby increasing photocatalytic hydrogen production, as illustrated in Figure 7f [101]. Similarly, in the GaN-ZnO oxynitride (hexagonal $P6_3mc$), HPT not only refines grains but also transforms detrimental native nitrogen monovacancies (acting as recombination centers) into nitrogen-based vacancy complexes [115]. This rearrangement of vacancies reduces radiative recombination, narrows the bandgap from 2.7 eV to 2.4 eV, elevates the conduction band energy

for a higher hydrogen evolution overpotential, and ultimately triples the photocatalytic hydrogen production rate. These studies demonstrate that a combination of high pressure and shear strain in HPT can deliberately engineer vacancy types and concentrations, converting defects from photocatalytic inhibitors into active and structure-modifying agents. A main difference between HPT and other methods used to produce vacancy-rich and black photocatalysts is that (i) HPT is a mechanical method and applies to any catalyst, and (ii) HPT offers a dopant-free alternative to chemical methods [111,112].

3.3.3. Composite and Heterojunction Photocatalysts

Composites with heterojunctions are an attractive group of photocatalysts that have received much attention in recent years [116,117]. The main interest in these catalysts lies in the fact that interphases between phases can enhance carrier separation and mobility, potentially improving charge carrier lifetime and photocatalysis [118,119]. HPT provides a one-step synthesis for composite photocatalysts with intimately mixed heterojunctions. Unlike conventional high-temperature or wet-chemical methods, HPT operates at room temperature, enabling the nanoscale integration of dissimilar semiconductor phases, such as TiO_2 with ZnO [102], CdS with TiO_2 [103], or P-type CuO with N-type $TiZrNbTaZnO_{10}$ [120] without undesirable phase reactions or the need for surfactants. The process simultaneously introduces high densities of lattice defects, including dual oxygen and sulfur vacancies [103], which can function as active sites and enhance the performance of heterojunctions [119]. Crucially, HPT induces grain refinement, promoting the formation of numerous clean interphase boundaries between the constituent materials. These boundaries act as effective heterojunctions (e.g., Type-II or Z-scheme), facilitating the spatial separation of photogenerated charge carriers, as evidenced by suppressed photoluminescence and enhanced photocurrent responses [117]. Furthermore, the applied pressure can trigger phase transformations, generating extra interphases between the polymorphs of the same material, such as in TiO_2 [102,117], ZnO [102] and CdS [117]. The synergistic integration of these features through a single HPT process results in composites with significantly boosted photocatalytic performance for diverse applications, including hydrogen production and oxygen generation [121].

3.3.4. High-Entropy Photocatalysts

High-entropy materials were first introduced with the concept of high-entropy alloys [122,123], but significant efforts are now focused on high-entropy ceramics, characterized by the incorporation of five or more principal cations into a single or dual-phase lattice [124,125]. The advent of high-entropy photocatalysts, first introduced in 2020 via HPT synthesis [104], represents a paradigm shift in the design of advanced functional materials for solar hydrogen production. Initial studies demonstrated that high-entropy oxide $TiZrHfNbTaO_{11}$ (monoclinic A2/m + orthorhombic Ima2) [104] and high-entropy oxynitride $TiZrHfNbTaO_6N_3$ (cubic $Fm\bar{3}m$ + orthorhombic P21/c) [105] with d^0 cationic configurations could be synthesized via HPT, exhibiting photocatalytic hydrogen evolution. It was suggested that these high-entropy photocatalysts benefit from the so-called cocktail effect, where the synergistic interaction of multiple elements leads to optimized light absorption, charge carrier separation, and surface reactivity [126]. Subsequent studies have expanded this concept by exploring the role of cationic electronic configurations, such as $d^0 + d^{10}$ [127,128], $d^{10} + s^0p^0$ [129] and $d^0 + d^{10} + s^0$ [130], in tuning the work function, band alignment, and vacancy formation in HEOs. For instance, the incorporation of alkali metals like cesium into high-entropy oxides has been shown to widen the electronegativity mismatch, enhance oxygen vacancy concentration, and improve photocatalytic performance for water splitting without the need for precious metal cocatalysts [130]. Density functional theory has shown that elements

with low electronegativity can enhance water adsorption on the surface, thereby enhancing hydrogen production [131]. The use of HPT to synthesize high-entropy perovskites also resulted in the development of photocatalysts that can produce hydrogen without the need for precious co-catalysts [132]. Figure 7g shows the structure of a high-entropy photocatalyst, modeled using first-principles calculations [131], and Figure 7h demonstrates the significance of cationic configuration of high-entropy oxides on their photocatalytic activity for hydrogen production [129]. Although the activity of HPT-synthesized high-entropy photocatalysts per catalyst surface area is among the highest ever reported, they suffer from a small surface area due to the effects of HPT and subsequent high-temperature calcination on the consolidation of powders [35,96]. To address this issue, laser crushing was used in a study [133], while many other studies attempted to use chemical methods to synthesize high-entropy photocatalysts for different reactions [134–136].

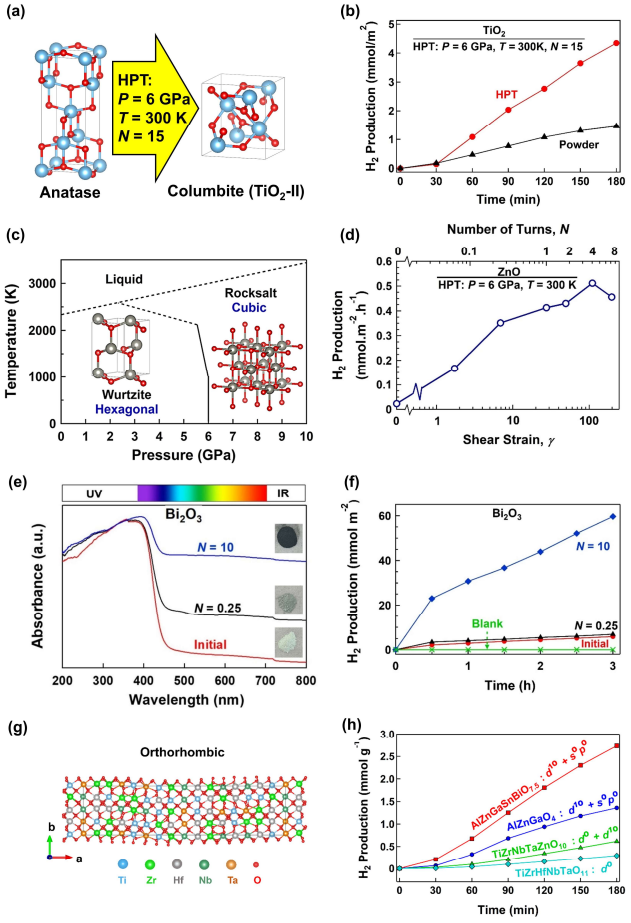


Figure 7. Enhanced photocatalytic hydrogen production by HPT processing. (**a**) Schematics of phase transformation from anatase to columbite in TiO_2 oxide by HPT processing [44], (**b**) hydrogen production versus illumination time for TiO_2 without and with HPT processing [44], (**c**) temperature–pressure phase diagram of ZnO oxide [54], (**d**) hydrogen production versus shear strain and number of HPT turns for ZnO [54], (**e**) light absorbance spectra of Bi_2O_3 oxide processed by HPT for 1/4 and 10 turns compared with the initial sample (inset: appearance of samples) [101], (**f**) hydrogen production versus time for Bi_2O_3 oxide processed by HPT for 1/4 and 10 turns compared with the initial sample [101], (**g**) simulated structure of Ti-Zr-Hf-Nb-Ta-O high-entropy oxide [131], and (**h**) hydrogen production versus time for high-entropy oxides with different cationic configurations [129].

3.4. Photoelectrocatalytic Hydrogen Production

Photoelectrocatalytic hydrogen production combines photocatalysis with electrochemical bias to enhance charge separation and suppress electron–hole recombination, thereby

improving hydrogen evolution efficiency [137,138]. In this approach, semiconductor photoelectrodes are illuminated under an applied potential, enabling directional transport of photogenerated charge carriers toward hydrogen evolution reactions [137,138]. High-entropy oxides have recently emerged as promising photoelectrocatalytic materials due to their tunable band structures, high structural stability, and abundant active sites. In a study, Ti-Zr-Hf-Nb-Ta-O high-entropy oxide was synthesized with the aid of HPT, and its performance as a photoanode for photoelectrocatalytic hydrogen generation from water was evaluated, as schematically shown in Figure 8a [139]. The band structure of the high-entropy oxide, which satisfies the required conditions for water splitting, is shown in Figure 8b [131]. Under xenon lamp irradiation and an applied bias of 0.7 V, it exhibited a hydrogen production rate of 1940 μmol cm^{-2} h^{-1}, surpassing that of the benchmark P25 TiO_2 catalyst, which was 1690 μmol cm^{-2} h^{-1}. Moreover, its activity for photocatalysis was much higher than that of conventional photocatalysts, as shown in Figure 8c [139]. The enhanced activity was attributed to the coexistence of monoclinic and orthorhombic phases forming heterojunctions, which facilitated charge separation, along with the presence of oxygen vacancies that improved charge mobility and light absorption. Notably, the high-entropy oxide also showed excellent reusability over multiple cycles without performance degradation [139]. This study highlights the potential of high-entropy ceramics as efficient, stable photoanodes for solar-driven hydrogen production, opening a new avenue for the application of entropy-stabilized materials in photoelectrocatalytic hydrogen production.

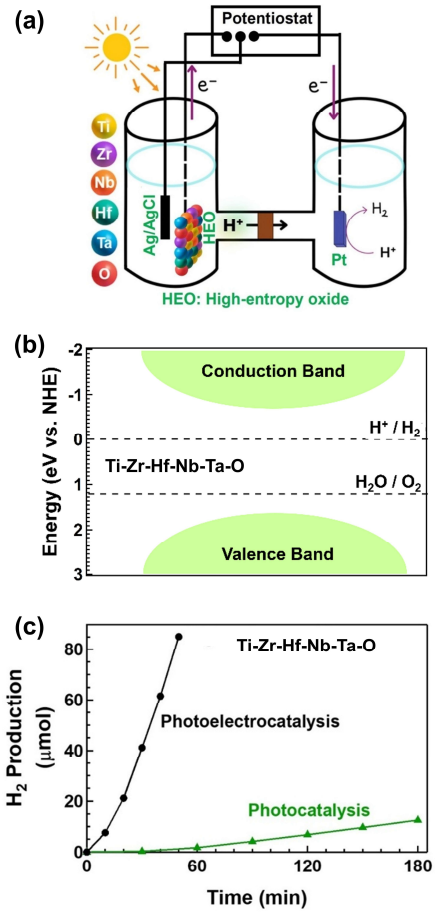


Figure 8. Enhanced photoelectrocatalytic hydrogen production through HPT processing. (**a**) Schematic illustration of a photoelectrocatalytic cell with Ti-Zr-Hf-Nb-Ta-O high-entropy oxide as photoanode [139], (**b**) band structure of Ti-Zr-Hf-Nb-Ta-O [131], and (**c**) hydrogen production versus time using the Ti-Zr-Hf-Nb-Ta-O photoelectrocatalyst compared to the same oxide as only photocatalyst [139].

3.5. Hydrogen Production by Photoreforming of Plastic Waste

The photoreforming of plastic waste into hydrogen is a promising dual-purpose strategy that addresses both environmental plastic pollution and clean energy needs [140]. A wide range of catalysts, including sulfides [141,142], nitrides [143,144], phosphides [145,146], and oxides [147,148], have been used for this nature-friendly process. Recent research has demonstrated the significant role of catalyst engineering by HPT in enhancing this process, particularly in degrading polar plastics such as polyethylene terephthalate (PET). HPT-synthesized high-entropy catalysts, in particular, have shown exceptional performance in this regard. A Ti-Zr-Hf-Nb-Ta-based high-entropy oxide catalyst has been reported to efficiently reform PET, yielding hydrogen alongside valuable organic products like formic acid and acetic acid [149]. The catalytic enhancement is attributed to the unique electronic and structural properties of high-entropy materials, including lattice distortion and optimized band structures, which improve charge separation and light absorption [149]. The addition of nitrogen to this high-entropy oxide and the formation of a high-entropy oxynitride led to increased lattice distortion and photoreforming activity, as shown in Figure 9a,b [150]. Additionally, the stabilization of high-pressure phases, such as the columbite polymorph of TiO_2 through HPT, has further advanced the photoreforming of PET [151]. The hydrothermal process followed by the HPT approach was also used to introduce sulfur vacancies and phase transformation from hexagonal to cubic ($P6_3m$ to $F\bar{4}3m$) in CdS, significantly boosting hydrogen evolution, as shown in Figure 9c, and PET conversion into useful chemicals, as shown in Figure 9d [103].

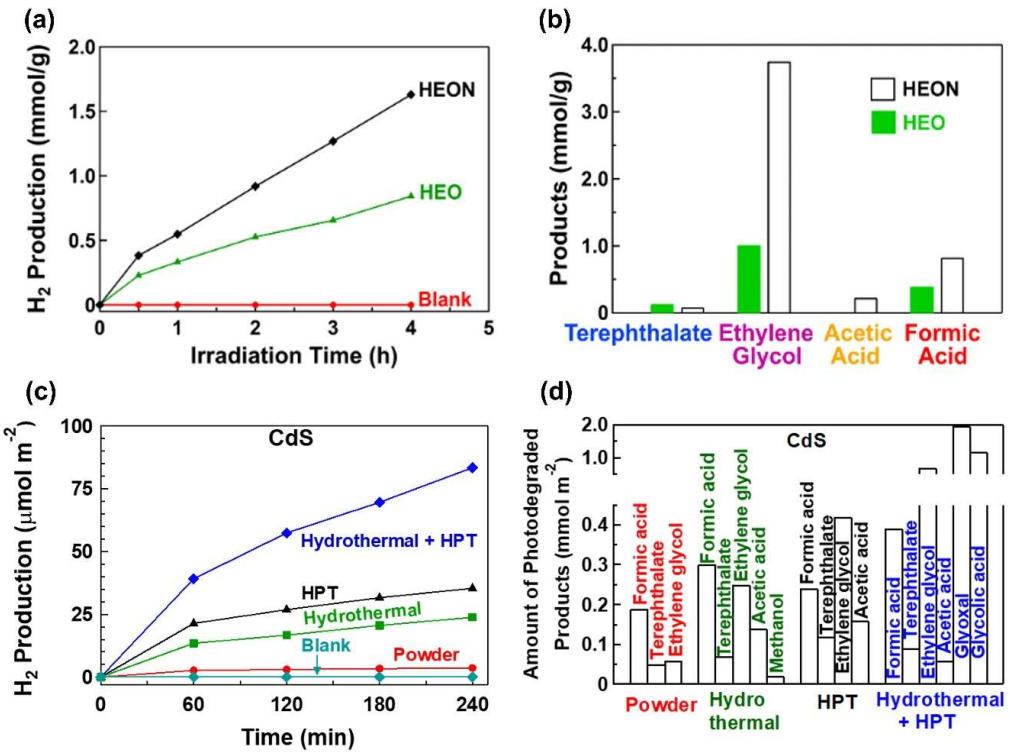


Figure 9. Enhanced hydrogen production via photoreforming of plastic waste using HPT processing. (**a**) Hydrogen production versus time and (**b**) organic product concentration during the photoreforming of PET plastic using $TiZrHfNbTaO_{11}$ high-entropy oxide (HEO) and $TiZrHfNbTaO_6N_3$ high-entropy oxynitride (HEON) synthesized by HPT [45]. (**c**) Hydrogen production versus time and (**d**) organic product concentration during the photoreforming of PET plastic using CdS processed by HPT, hydrothermal, and hydrothermal followed by HPT, including initial powder [150].

In contrast, the photoreforming of non-polar plastics such as polypropylene (PP) poses a greater challenge due to their chemical stability and hydrophobic nature [140]. To address this, mechanical pretreatment via HPT has been successfully applied to create intimately mixed composites of PP with photocatalysts such as brookite TiO_2 [152]. The HPT process induces structural defects and forms extensive inorganic-organic interfaces, which collectively enhance charge transfer and suppress recombination. As a result, hydrogen production from PP increases systematically with HPT processing, achieving multi-fold improvements over untreated mixtures [152]. Another strategy used for the pretreatment of PP plastic before photoreforming involves exposing it to sunlight for a long time to break its atomic bonds using UV light [153]. These strategies highlight the adaptability of HPT and other pretreatment strategies in overcoming the inherent stability of non-polar plastics, thereby extending the benefits of hydrogen production from PET photoreforming to a wider range of plastic wastes.

4. Implication of High-Pressure Torsion for Hydrogen Storage

Solid-state hydrogen storage using metals and alloys remains a promising yet challenging approach due to limitations associated with difficult activation, slow kinetics, and unfavorable thermodynamics [6,7]. Severe plastic deformation methods, such as equal-channel angular pressing [154–158], rolling-based techniques [159–163], forging-based techniques [164–168], and HPT [169–173], have been widely used to process hydrogen storage materials. Among these methods, it has been proven that HPT is a highly effective processing route for overcoming these challenges by enabling extreme grain refinement and the introduction of high densities of lattice defects in metals [174–176], alloys [177–179], intermetallics [180–182], amorphous compounds [183–185], medium/high-entropy compounds [186–188] and composites [189–191]. Moreover, HPT allows for stabilization of metastable phases [38,53] and forces atomic-scale mixing of elements to form new hydrogen storage alloys in miscible systems [55,192] or even in immiscible binary [193,194], ternary [56,195] and high-entropy [196] systems. Early studies on HPT-processed hydrogen storage materials, including the first contribution of the current author to the field [197], primarily focused on kinetic enhancement. The power of HPT in solving the activation problem of hydrogen storage materials, particularly TiFe [198], made the process more popular for activation [199]. However, motivated by a study on the successful synthesis of an intermetallic by HPT [200], subsequent systematic investigations revealed that synthesis by HPT can be used as a materials design tool to tune hydrogen–metal interactions, ultimately enabling reversible hydrogen storage at room temperature in carefully designed systems [56]. The effect of HPT on the activation, kinetics, and thermodynamics of hydrogen storage materials, which are partly reviewed in a few publications [201–204], is discussed in this section.

4.1. Activation and Air Resistance Aspects

One of the most immediate and widely observed effects of HPT on hydrogen storage materials is the dramatic improvement in activation behavior. Many technologically relevant hydrides and intermetallic compounds suffer from surface oxide layers and low hydrogen diffusivity, resulting in difficult activation and long incubation times during the first hydrogenation cycle [205–207]. HPT effectively addresses these limitations by producing ultrafine-grained or nanocrystalline microstructures with exceptionally high grain boundary densities [180], dislocations [199], stacking faults [40], and partial amorphization [52]. The formation of grain boundaries after HPT provides a fast diffusion pathway for hydrogen and serves as a preferential site for hydride nucleation [180]. For TiFe-based intermetallics, which are well known for their poor activation behavior [205,206], HPT enables hydrogen absorption at room temperature without conventional activation treat-

ments such as high-temperature treatment or hydrogen cycling [198]. This behavior has been attributed to the effect of nanograin boundaries, partial amorphization, and cracks on hydrogen transport through the oxide layer [180]. The HPT-processed TiFe samples remain active for hydrogenation even after prolonged exposure to air (e.g., 400 days), confirming the significant improvement in air resistivity [198].

Similar activation has been reported in Ti-Fe-Mn intermetallics, as shown in Figure 10a [52], Ti-V alloys [199], and Ti-V-Cr alloys [179] processed by HPT, although hydrogen storage reversibility is negatively influenced by a large density of lattice defects in Ti-V-Cr [178]. HPT-assisted activation has also been demonstrated in medium-entropy alloys [188] and high-entropy alloys [177], where HPT further accelerates hydrogen uptake by refining grains, increasing defect-assisted diffusion pathways, and promoting homogeneous hydrogen distribution. Most of these HPT-processed hydrogen storage materials are air-resistant and can be kept in an air atmosphere for a long time without losing their activity [201,204]. Collectively, these studies establish HPT as one of the most effective routes for activating hydrogen storage materials. The knowledge achieved from the effect of grain boundaries on activation of HPT-processed and ball-milled hydrogen storage materials [208] has been recently used to activate high-entropy alloys using interphase boundaries [209]. Since HPT can affect the distribution of second-phase particles in different materials [210,211], its application to dual-phase hydrogen storage materials is expected to have a more significant effect on activation.

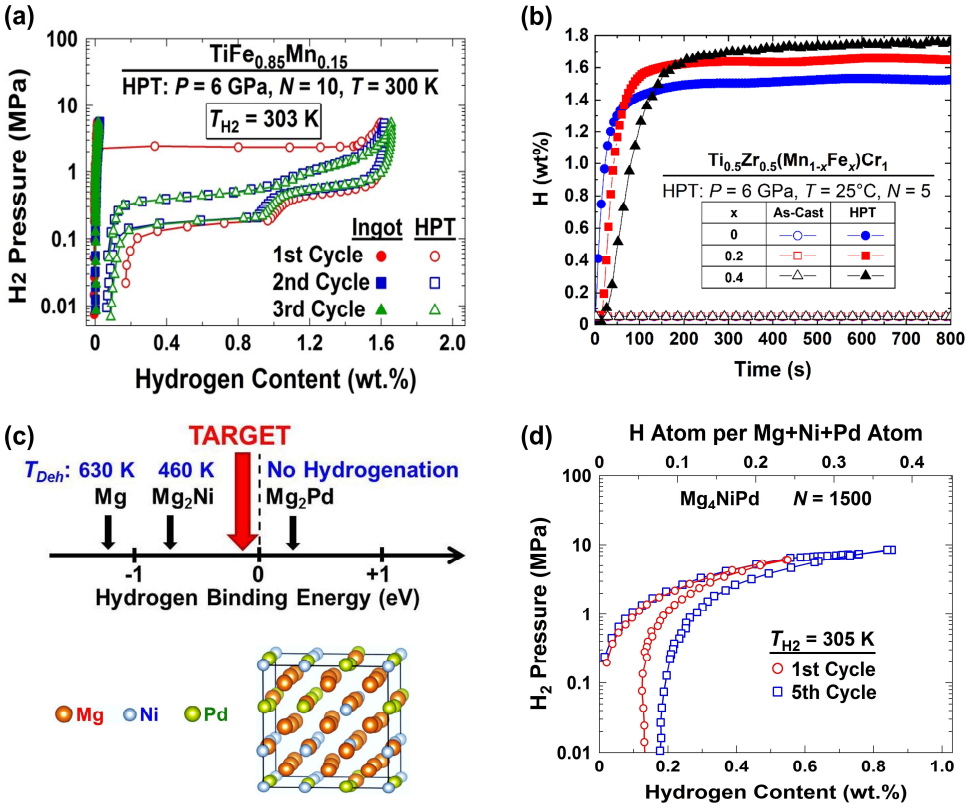


Figure 10. Enhanced hydrogen storage activation, kinetics, and thermodynamics through HPT processing. (**a**) Pressure–composition isotherms at room temperature for $TiFe_{0.85}Mn_{0.15}$ intermetallic after HPT processing compared to the initial ingots [52], (**b**) hydrogen storage versus time at room temperature for $Ti_{0.5}Zr_{0.5}Mn_{1-x}Fe_xCr_1$ (x = 0, 0.2, and 0.4) high-entropy alloys after HPT processing compared to the initial ingots [187], (**c**) the concept of hydrogen binding energy used to design Mg_4NiPd alloy with its simulated lattice structure [56], and (**d**) pressure–composition isotherms at room temperature for Mg_4NiPd synthesized by HPT processing [56].

4.2. Kinetic Aspects

Beyond activation, HPT significantly enhances hydrogenation and dehydrogenation kinetics [201–204]. Many hydrogen storage materials suffer from slow hydrogen absorption/desorption rates due to limited hydrogen diffusion and nucleation sites [212,213]. HPT effectively addresses these kinetic limitations by producing nanocrystalline structures and high defect densities without the need for a catalyst [201–204]. In magnesium, HPT reduces hydrogenation time and significantly accelerates hydrogen absorption kinetics compared with coarse-grained counterparts [197]. It was shown that low-angle grain boundaries are not as effective as high-angle grain boundaries in the hydrogenation of magnesium [197]. The effect of stacking faults on hydrogen storage performance was also investigated in Mg_2Ni intermetallics processed by HPT, confirming that stacking faults can be as effective as grain boundaries in enhancing hydrogenation kinetics [40]. Enhancement of kinetics by partial amorphization and formation of grain boundary was also reported in Ti-Fe-Mn intermetallics [52]. The kinetic enhancement by HPT has also been demonstrated in complex multi-component systems. For example, HPT-processed Laves phase high-entropy alloys exhibited very fast hydrogen absorption at room temperature even after prolonged air exposure, as shown in Figure 10b [187]. In a medium-entropy alloy with a body-centered cubic (BCC $Im\bar{3}m$) structure, it was found that HPT-induced dislocations and vacancies function as hydrogen trapping sites, while grain boundaries facilitate hydrogen transport during hydrogenation/dehydrogenation because of their larger free volumes [188]. These studies highlight the ability of HPT to overcome kinetic barriers through defect engineering and microstructural refinement.

4.3. Thermodynamic Aspects

While HPT is highly effective in improving activation and kinetics, achieving reversible hydrogen storage at near-ambient conditions also requires favorable thermodynamics [212,213]. Hydrogen binding energy determines equilibrium pressures, plateau characteristics, and desorption temperatures, governing the feasibility of practical hydrogen storage [16,17]. Although the effect of HPT on hydrogen thermodynamics can be minor via extreme lattice distortion, residual strain, and nanograin formation, the method has been used successfully to synthesize novel hydrogen storage materials with appropriate thermodynamics. HPT-induced metastable phases play a central role in thermodynamic tuning. For instance, the stabilization of the high-pressure γ-MgH_2 phase by HPT resulted in a decrease in dehydrogenation temperature by 80 K compared to conventional α-MgH_2 [53]. These metastable phases often have lower formation energy and thermodynamic stability under ambient conditions, resulting in reduced hydride stability and smoother hydrogen release at low temperatures [53].

A major conceptual advance was the use of HPT in ultra-severe plastic deformation regimes to force atomic-scale mixing even in miscible systems, thereby creating non-equilibrium environments with good hydrogen affinity [25,26,65]. In particular, Mg-Ni-Pd-based materials synthesized by HPT exhibit hydrogen binding energies that lie between those of magnesium and palladium hydrides, enabling reversible hydrogen absorption and desorption at room temperature, provided the composition is tuned for appropriate binding energy [56]. The metastable Mg_4NiPd phase (cubic $Im\bar{3}m$), designed using first-principles calculations (Figure 10c) and synthesized by HPT, exhibited reversible room-temperature hydrogen storage, as shown in Figure 10d, clearly demonstrating that HPT can be used to design hydrogen storage materials based on hydrogen binding energy engineering [56]. The TiZrCrMnFeNi alloy (hexagonal $P6_3/mmc$ + cubic $Pm\bar{3}m$), which exhibits fast and reversible hydrogen storage at room temperature, was also originally designed using concepts developed using the HPT method [186]. Despite the good thermodynamics and

reversibility of these phases at room temperature, their binding energy engineering should be conducted by employing theoretical calculations and/or machine learning.

5. Implication of High-Pressure Torsion for Hydrogen Embrittlement Resistance

Hydrogen embrittlement (deterioration of mechanical properties in the presence of hydrogen) is another significant challenge in the development of hydrogen as a clean fuel [214,215]. The effect of HPT on hydrogen embrittlement resistance is complex and material-dependent. This chapter reviews findings from key studies on various material systems, including low-carbon steels [216,217], austenitic stainless steels [218–220], twinning-induced plasticity (TWIP) steels [39], high-entropy alloys [41,221,222], and palladium [223], to elucidate the role of HPT in either mitigating or exacerbating hydrogen embrittlement.

5.1. Low-Carbon Steels

In ultra-low-carbon steels, HPT can produce submicrocrystalline structures that significantly increase strength but often at the expense of hydrogen embrittlement resistance. For instance, Todaka et al. demonstrated that submicrocrystalline ultra-low-carbon steel produced by HPT exhibited reduced ductility under hydrogen charging compared to its coarse-grained counterpart, highlighting the challenge of balancing strength and hydrogen embrittlement resistance in ferritic BCC systems [216]. Similarly, Mine et al. reported that an ultrafine-grained Fe–0.01C (wt%) alloy processed by HPT showed considerable strengthening but suffered from hydrogen-assisted cracking, suggesting that the high density of grain boundaries introduced by severe plastic deformation can act as pathways for hydrogen diffusion and sites for crack initiation [217].

5.2. Austenitic Stainless Steels

Austenitic stainless steels, with their face-centered cubic (FCC $Fm\bar{3}m$) structure, generally exhibit better hydrogen embrittlement resistance than ferritic BCC steels [214,215]. HPT processing of these steels refines the grain structure to ultrafine or nano scales, which can have contrasting effects. Mine et al. showed that HPT-processed Type 304 stainless steel could achieve high strength, but its hydrogen embrittlement resistance was highly sensitive to subsequent annealing treatments [218]. Annealing after HPT could restore some ductility under hydrogen by reducing dislocation density and possibly allowing the formation of more stable microstructures [218]. In a later study, they further clarified that ultrafine-grained austenitic stainless steels processed by HPT at moderate temperatures could exhibit a combination of high strength and retained, though reduced, resistance to hydrogen embrittlement [219]. The dense grain boundaries enhance hydrogen diffusion, but the inherent plasticity of the austenitic phase can help accommodate strain, preventing catastrophic failure [220].

5.3. Twinning-Induced Plasticity (TWIP) Steels

The effect of HPT on nanotwinned TWIP steels presents a complex picture [39]. As demonstrated by Mohammadi et al., introducing a nanotwinned austenitic structure in an Fe-23Mn-0.5C (wt%) TWIP steel via HPT followed by annealing led to a high tensile strength (~1.4 GPa) but resulted in a complete loss of ductility after hydrogen charging [39]. The fracture surfaces revealed quasi-cleavage features with step-like ridges, indicating that twin boundaries acted as preferential sites for crack initiation and propagation in a hydrogen atmosphere. This finding contrasted with the HPT-processed but unannealed sample, which had a bimodal martensitic structure and retained ~6% uniform ductility under hydrogen. The study concluded that in TWIP steels, pre-existing nanotwins introduced by

HPT followed by annealing are detrimental to hydrogen embrittlement resistance, as they facilitate crack propagation faster than dislocation accumulation [39].

5.4. High-Entropy Alloys

High-entropy alloys, particularly FCC CrMnFeCoNi (Cantor alloy), have emerged as promising candidates for hydrogen-compatible applications due to their inherent resistance to hydrogen embrittlement [224–226]. HPT processing to high strains (e.g., 10 turns) produces nanograins (~25 nm) in CrMnFeCoNi, leading to ultra-high yield strength (>1900 MPa). However, this comes with catastrophic hydrogen embrittlement, causing failure in the elastic region after hydrogen charging [221]. The high density of grain boundaries facilitates massive hydrogen uptake (up to 27 wt. ppm) and promotes intergranular cracking via the hydrogen-enhanced decohesion mechanism (HEDE). At lower HPT strains, where the microstructure contains a high density of deformation twins and sessile dislocation structures (e.g., Lomer–Cottrell locks and D-Frank partial dislocations), a superior combination is achieved [41]. For instance, after 1/8–1/4 HPT turns, the Cantor alloy exhibited high yield strength (>1 GPa) and retained significant ductility (up to 9%) under hydrogen. These defects act as potent barriers, pinning dislocation motion and suppressing the hydrogen-enhanced localized plasticity (HELP) mechanism. The best combination of strength (2 GPa) and hydrogen embrittlement resistance (10% plasticity) was achieved for an HPT-processed $Al_{0.1}$CrFeCoNi alloy, in which aluminum diminishes hydrogen diffusion from the surface to the bulk [222]. As shown in Figure 11a, this alloy can break the strength and plasticity trade-off under hydrogen [222].

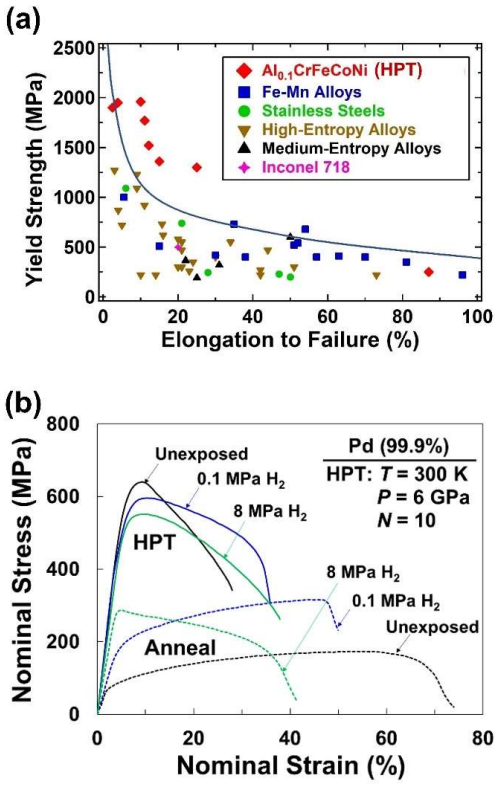


Figure 11. Enhanced strength and hydrogen embrittlement resistance synergy through HPT processing. (**a**) Variation of strength versus elongation to failure for $Al_{0.1}$CrfeCoNi high-entropy alloy processed using different HPT turns compared to reported data and other alloys in the presence of hydrogen [222], and (**b**) influence of hydrogen charging at two different pressures on the stress–strain curves of palladium in coarse-grained annealed condition and ultrafine-grained HPT-processed condition [223].

5.5. Palladium

Palladium offers a unique case study where HPT-induced grain refinement fundamentally alters the hydrogen-material interaction from embrittlement to softening. Hongo et al. showed that coarse-grained palladium hardened and became embrittled upon hydrogen exposure due to hydride formation [223]. In stark contrast, HPT-processed palladium with an average grain size of 220 nm exhibited hydrogen-induced softening and enhanced plasticity, as shown in Figure 11b [223]. The ultra-high dislocation density in the saturated ultrafine-grained microstructure interacts with hydrogen via the HELP mechanism, where hydrogen enhances dislocation mobility, reducing flow stress and increasing tensile ductility [223]. This reversal of behavior underscores the critical role of the initial defect state in determining whether hydrogen will be detrimental (via HEDE/hydride formation) or beneficial (via HELP) to mechanical performance [10,11].

5.6. Criteria for Predicting Hydrogen Embrittlement

Due to differences in hydrogen embrittlement mechanisms in different materials and limited publications on the effect of HPT on this phenomenon, it is hard to find a universal criterion to predict the behavior of HPT-treated materials. However, the contrasting effects of HPT on hydrogen embrittlement can be rationalized by at least three microstructural criteria. (i) The grain size regime is the most critical [227,228]: HPT-driven grain refinement to the nanoscale (<100 nm) typically worsens hydrogen embrittlement resistance by creating an excessive density of high-angle grain boundaries [216–222]. These boundaries act as fast diffusion pathways for hydrogen and weak interfaces for crack initiation via the HEDE mechanism [10,11]. A moderate ultrafine-grained structure with sizes of 100–1000 nm offers a better balance, provided the boundary character and other defects are optimized [218–220]. (ii) The nature of defects is more critical than their density. For example, HPT improves resistance when it introduces coherent, low-energy barriers like deformation twins [226], which suppress dislocation slip via the HELP mechanism [10,11]. However, boundaries worsen resistance when they are incoherent with high-energy interfaces, as they can serve as preferential crack paths [216,217]. (iii) Dislocation mobility has a complex effect on embrittlement and hydrogen accumulation [229]. In unique cases of palladium, an ultra-high density of mobile dislocations by HPT treatment allows hydrogen to enhance plasticity, reversing embrittlement via the HELP mechanism [223]. However, typically, a high density of immobile or sessile dislocations, like Lomer–Cottrell locks and D-Frank partial dislocations, is beneficial for high strength and good hydrogen embrittlement resistance [221,222].

6. Issues with High-Pressure Torsion

While severe plastic deformation methods, particularly HPT, are widely used for fundamental studies and materials design, there has been limited success in their commercialization, mainly in the biomaterials sector [230]. Two major issues with the commercialization of these methods are (i) making the methods continuous [231] and (ii) scaling up the sample size [232]. For processing metallic materials, methods like accumulative roll bonding [233,234] and equal-channel angular pressing—conform [235,236] can be feasibly used to produce rather large samples in a continuous process. However, for processing hard and brittle materials, where high pressure is needed, HPT is still the main process [237]. Although HPT is mainly employed as a tool for fundamental studies and the design of new materials in the hydrogen sector, there have been some attempts to scale up the HPT [238] method or make it continuous [29]. The main attempts include (i) using high-capacity hydrolytic presses (e.g., 1000 tons) [239], and (ii) developing modified HPT methods, such as HPT with bulk samples [240], HPT with ring samples [28], continuous HPT [29], incre-

mental HPT [241], planar HPT [242], high-pressure torsion extrusion [243], high-pressure tube twisting [244], tube high-pressure shearing [245], high-pressure sliding [246], etc.

The thermal and operational stability of highly defective and severely deformed materials, including those processed by HPT, is another critical issue [247,248]. At ambient temperature, these materials exhibit high stability, although there are reports of microstructural changes over time in pure metals or alloys with low melting temperatures after HPT [249,250]. Materials used for hydrogen production and embrittlement resistance are generally used at ambient temperature and exhibit high stability. Moreover, materials like TiFe [180,181] or Mg_4NiPd [57], which are used for hydrogen storage at room temperature, are quite stable [201]. While HPT-processed materials can suffer from structural relaxation at elevated temperatures, their stability can be improved by solute atoms or the generation of composite structures [251,252]. For example, during hydrogen storage, even at high temperatures, they still exhibit remarkable cyclic stability [202]. Significant research efforts have demonstrated that although defect density may decrease, severely deformed hydrogen storage materials retain a superior density of grain boundaries and lattice imperfections compared to their conventional coarse-grained counterparts, even after prolonged exposure [173]. Consequently, their enhanced hydrogen storage kinetics and capacity often remain significantly improved over hundreds, and in some cases up to a thousand, thermal cycles at high operational temperatures (like 423 K for magnesium alloys) [253,254].

Another issue with the use of HPT is the consolidation of powders. While this issue is positively used to produce bulk nanostructured samples of metallic or metal-based composite materials [255,256], it generates some problems for HPT-processed catalysts, such as high-entropy photocatalysts [97]. A large surface area is a major requirement for catalysts [257], but the consolidation of powders undesirably reduces the final surface area of even oxides and ceramics [35,96]. So far, there has been an attempt to increase the surface area by post-HPT laser crushing [133]. Future studies are expected to consider using mechanical methods, such as ball milling (although the method may affect structural and microstructural features) [258,259] or chemical methods, such as etching [260,261], to produce nanopowders or porous powders from HPT-treated catalysts. In general, combining severe plastic deformation with other mechanical, chemical, and thermal methods is expected to promote the production of hybrid materials with a good synergy of properties.

The presence of a variety of defects after HPT and their different roles in hydrogen-related applications is another issue. HPT simultaneously generates a wide range of defects, such as vacancies, dislocations, and grain boundaries [262,263], and thus, all these defects affect the final properties [21–25]. For example, grain boundaries are beneficial for hydrogen storage [201], but dislocations may destroy reversibility [178,179]. Vacancies and dislocations are advantageous for photocatalysis [264,265], but grain boundaries may negatively affect photocatalysis, although there are also reports on the positive effect of grain boundaries on photocatalysis [266,267]. Grain boundaries are not appropriate for hydrogen embrittlement (although necessary to achieve high strength), but twins and sessile dislocation-based defects are desirable for hydrogen storage [216–222]. Since the type and fraction of defects can be somehow controlled by combining severe plastic deformation with pre- or post-thermal treatment [268,269], future studies should consider optimizing defects for specific applications.

7. Concluding Remarks and Future Prospects

High-pressure torsion (HPT) has evolved from a foundational method in severe plastic deformation into a transformative, multi-purpose platform for designing and engineering materials for the entire hydrogen value chain. This review demonstrates that the capacity

of HPT to generate extreme shear strains under high pressure enables unprecedented microstructural and compositional control, directly addressing the core challenges in hydrogen production, storage, and hydrogen embrittlement resistance. The ability of HPT to introduce dense, tunable defect populations (vacancies, dislocations, Lomer–Cottrell locks, D-Frank partial dislocations, stacking faults, twins, and grain boundaries) and to synthesize novel materials and non-equilibrium phases (high-pressure polymorphs, amorphous regions, and high-entropy compounds) provides a versatile toolkit for tailoring hydrogen-related properties. For hydrogen production, HPT facilitates the creation of highly active, vacancy-rich, and compositionally complex compounds for hydrolysis, electrocatalysis, photocatalysis, photoelectrocatalysis, and photoreforming, particularly establishing high-entropy oxides and oxynitrides as a new class of photocatalysts. For hydrogen storage, HPT not only solves long-standing activation and kinetic problems but also, through strategic materials synthesis, enables the design of systems with thermodynamically favorable hydrogen binding energies for reversible room-temperature storage. For hydrogen embrittlement resistance, HPT reveals a complex interplay between microstructure and hydrogen damage, demonstrating that defect engineering can either mitigate (through dislocation pinning and strain delocalization) or exacerbate (via accelerated hydrogen diffusion) embrittlement, depending on the material system and dominant failure mechanism.

Although HPT is still used at the laboratory scale for fundamental studies, it has high potential to be used for hydrogen production, storage, and compatibility applications. Future research should focus on several key directions to fully employ the potential of HPT: establishing predictive structure–property relationships through integrated in-situ characterization and multiscale modeling; transitioning from laboratory synthesis to scalable manufacturing via continuous shear-based processes and hybrid techniques; designing multifunctional materials that combine structural, catalytic, and storage capabilities; expanding the exploration of entropy-stabilized and metastable compounds into new compositional spaces; and rigorously assessing long-term durability under real-world operating conditions to ensure practical application. As the demand for carbon-neutral energy solutions intensifies, the continued advancement and intelligent application of severe plastic deformation, with HPT at its forefront, will be critical in developing the high-performance materials necessary to realize a safe, efficient, and sustainable hydrogen economy.

Funding: This research received no external funding.

Data Availability Statement: No new data were created or analyzed in this study.

Conflicts of Interest: The author declares no conflicts of interest.

References

1. Züttel, A.; Borgschulte, A.; Schlapbach, L. *Hydrogen as a Future Energy Carrier*; Wiley VCH Verlag GmbH & Co.: Weinheim, Germany, 2008.
2. Staffell, I.; Scamman, D.; Abad, A.V.; Balcombe, P.; Dodds, P.E.; Ekins, P.; Shah, N.; Ward, K.R. The role of hydrogen and fuel cells in the global energy system. *Energy Environ. Sci.* **2019**, *12*, 463–491.
3. Yue, M.; Lambert, H.; Pahon, E.; Roche, R.; Jemei, S.; Hissel, D. Hydrogen energy systems: A critical review of technologies, applications, trends and challenges. *Renew. Sustain. Energy Rev.* **2021**, *146*, 111180. [CrossRef]
4. Iulianelli, A.; Liguori, S.; Wilcox, J.; Basile, A. Advances on methane steam reforming to produce hydrogen through membrane reactors technology: A review. *Catal. Rev. Sci. Eng.* **2016**, *58*, 1–35. [CrossRef]
5. Capa, A.; Yan, Y.; Rubiera, F.; Pevida, C.; Gil, M.V.; Clough, P.T. Process simulations of high-purity and renewable clean H_2 production by sorption enhanced steam reforming of biogas. *ACS Sustain. Chem. Eng.* **2023**, *11*, 4759–4775. [CrossRef]
6. Von Colbe, J.B.; Ares, J.R.; Barale, J.; Baricco, M.; Buckley, C.; Capurso, G.; Gallandat, N.; Grant, D.M.; Guzik, M.N.; Jacob, I.; et al. Application of hydrides in hydrogen storage and compression: Achievements, outlook and perspectives. *Int. J. Hydrogen Energy* **2019**, *44*, 7780–7808. [CrossRef]

7. Hirscher, M.; Yartys, V.A.; Baricco, M.; Bourgeois, N.; Buckley, C.E.; Colbe, J.M.B.V.; Crivello, J.C.; Cuevas, F.; Denys, R.V.; Dornheim, M.; et al. Materials for hydrogen-based energy storage—Past, recent progress and future outlook. *J. Alloys Compd.* **2020**, *827*, 153548.
8. Singla, M.K.; Nijhawan, P.; Oberoi, A.S. Hydrogen fuel and fuel cell technology for cleaner future: A review. *Environ. Sci. Pollut. Res.* **2021**, *28*, 15607–15626. [CrossRef] [PubMed]
9. Hwang, J.; Maharjan, K.; Cho, H. A review of hydrogen utilization in power generation and transportation sectors: Achievements and future challenges. *Int. J. Hydrogen Energy* **2023**, *48*, 28629–28648. [CrossRef]
10. Dwivedi, S.K.; Vishwakarma, M. Hydrogen embrittlement in different materials: A review. *Int. J. Hydrogen Energy* **2018**, *43*, 21603–21616. [CrossRef]
11. Martin, M.L.; Dadfarnia, M.; Nagao, A.; Wang, S.; Sofronis, P. Enumeration of the hydrogen-enhanced localized plasticity mechanism for hydrogen embrittlement in structural materials. *Acta Mater.* **2019**, *165*, 734–750. [CrossRef]
12. Gabriel, K.S.; El-Emam, R.S.; Zamfirescu, C. Technoeconomics of large-scale clean hydrogen production—A review. *Int. J. Hydrogen Energy* **2022**, *47*, 30788–30798. [CrossRef]
13. Zainal, B.S.; Ker, P.J.; Mohamed, H.; Ong, H.C.; Fattah, I.M.R.; Rahman, S.M.A.; Nghiem, L.D.; Mahlia, T.M.I. Recent advancement and assessment of green hydrogen production technologies. *Renew. Sustain. Energy Rev.* **2024**, *189*, 113941. [CrossRef]
14. Liu, W.; Sun, L.; Li, Z.; Fujii, M.; Geng, Y.; Dong, L.; Fujita, T. Trends and future challenges in hydrogen production and storage research. *Environ. Sci. Pollut. Res.* **2020**, *27*, 31092–31104. [CrossRef] [PubMed]
15. Kumar, R.; Singh, R.; Dutta, S. Advances in materials and systems for hydrogen production and storage: A review. *Energy Fuels* **2024**, *38*, 2601–2629. [CrossRef]
16. Pasquini, L.; Sakaki, K.; Akiba, E.; Allendorf, M.D.; Alvares, E.; Ares, J.R.; Babai, D.; Baricco, M.; von Colbe, J.B.; Bereznitsky, M.; et al. Magnesium- and intermetallic alloys-based hydrides for energy storage: Modelling, synthesis and properties. *Prog. Energy* **2022**, *4*, 032007. [CrossRef]
17. Yartys, V.A.; Lototskyy, M.V.; Akiba, E.; Albert, R.; Antonov, V.E.; Ares, J.R.; Baricco, M.; Bourgeois, N.; Buckley, C.E.; Bellosta von Colbe, J.M.; et al. Magnesium based materials for hydrogen based energy storage: Past, present and future. *Int. J. Hydrogen Energy* **2019**, *44*, 7809–7859. [CrossRef]
18. Pasquini, L. Design of nanomaterials for hydrogen storage. *Energies* **2020**, *13*, 3503. [CrossRef]
19. Yu, H.; Díaz, A.; Lu, X.; Sun, B.; Ding, Y.; Koyama, M.; He, J.; Zhou, X.; Oudriss, A.; Feaugas, X.; et al. Hydrogen embrittlement and fatigue of structural materials: A review. *Chem. Rev.* **2024**, *124*, 6271–6392.
20. Campari, A.; Ustolin, F.; Alvaro, A.; Paltrinieri, N. A review on hydrogen embrittlement and risk-based inspection of hydrogen technologies. *Int. J. Hydrogen Energy* **2023**, *48*, 35316–35346. [CrossRef]
21. Valiev, R.Z.; Islamgaliev, R.K.; Alexandrov, I.V. Bulk nanostructured materials from severe plastic deformation. *Prog. Mater. Sci.* **2000**, *45*, 103–189. [CrossRef]
22. Valiev, R.Z.; Estrin, Y.; Horita, Z.; Langdon, T.G.; Zehetbauer, M.J.; Zhu, Y. Producing bulk ultrafine-grained materials by severe plastic deformation: Ten years later. *JOM* **2016**, *68*, 1216–1226. [CrossRef]
23. Zhilyaev, A.P.; Langdon, T. Using high-pressure torsion for metal processing: Fundamentals and applications. *Prog. Mater. Sci.* **2008**, *53*, 893–979. [CrossRef]
24. Edalati, K.; Horita, Z. A review on high-pressure torsion (HPT) from 1935 to 1988. *Mater. Sci. Eng. A* **2016**, *652*, 325–352. [CrossRef]
25. Edalati, K. Metallurgical alchemy by ultra-severe plastic deformation via high-pressure torsion process. *Mater. Trans.* **2019**, *60*, 1221–1229. [CrossRef]
26. Kilmametov, A.; Kulagin, R.; Mazilkin, A.; Seils, S.; Boll, T.; Heilmaier, M.; Hahn, H. High-pressure torsion driven mechanical alloying of CoCrFeMnNi high entropy alloy. *Scr. Mater.* **2019**, *158*, 29–33. [CrossRef]
27. Bridgman, P.W. Effects of high shearing stress combined with high hydrostatic pressure. *Phys. Rev.* **1935**, *48*, 825–847. [CrossRef]
28. Harai, Y.; Edalati, K.; Horita, Z.; Langdon, T.G. Using ring samples to evaluate the processing characteristics in high-pressure torsion. *Acta Mater.* **2009**, *57*, 1147–1153. [CrossRef]
29. Edalati, K.; Horita, Z. Continuous high-pressure torsion. *J. Mater. Sci.* **2010**, *45*, 4578–4582. [CrossRef]
30. Starink, M.J.; Cheng, X.; Yang, S. Hardening of pure metals by high-pressure torsion: A physically based model employing volume-averaged defect evolutions. *Acta Mater.* **2013**, *61*, 183–192.
31. Han, J.K.; Jang, J.I.; Langdon, T.G.; Kawasaki, M. Bulk-state reactions and improving the mechanical properties of metals through high-pressure torsion. *Mater. Trans.* **2019**, *60*, 1131–1138. [CrossRef]
32. Hosokawa, A.; Ohtsuka, H.; Li, T.; Ii, S.; Tsuchiya, K. Microstructure and magnetic properties in nanostructured Fe and Fe-based intermetallics produced by high-pressure torsion. *Mater. Trans.* **2014**, *55*, 1286–1291.
33. Volkova, E.G.; Valiullin, A.I.; Pilyugin, V.P.; Tolmachev, T.P.; Livinets, A.A.; Gavrilova, A.A.; Gurianov, D.A.; Volkov, A.Y. Formation of intermetallic Al_2Pt-phase by high pressure torsion of elemental chips at cryogenic temperature. *Met. Mater. Int.* **2025**, *31*, 2057–2068.

34. Levitas, V.I. Strain-induced phase transformations, chemical reactions, microstructure evolution, and severe plastic deformations under high pressure. *Prog. Mater. Sci.* **2026**, *158*, 101625.
35. Edalati, K.; Hidalgo-Jiménez, J.; Nguyen, T.T.; Sena, H.; Enikeev, N.; Rogl, G.; Levitas, V.I.; Horita, Z.; Zehetbauer, M.J.; Valiev, R.Z.; et al. Severe plastic deformation of ceramics by high-pressure torsion: Review of principles and applications. *Annu. Rev. Mater. Res.* **2025**, *55*, 89–124. [CrossRef]
36. Révész, Á.; Spassov, T.; Kis, V.K.; Schafler, E.; Gajdics, M. The influence of preparation conditions on the hydrogen sorption of Mg-Nb_2O_5-CNT produced by ball milling and subsequent high-pressure torsion. *J. Nanosci. Nanotechnol.* **2020**, *20*, 4587–4590. [PubMed]
37. Gajdics, M.; Spassov, T.; Kis, V.K.; Béke, F.; Novák, Z.; Schafler, E.; Révész, Á. Microstructural investigation of nanocrystalline hydrogen-storing Mg-titanate nanotube composites processed by high-pressure torsion. *Energies* **2020**, *13*, 563.
38. Kitabayashi, K.; Edalati, K.; Li, H.W.; Akiba, E.; Horita, Z. Phase transformations in MgH_2-TiH_2 hydrogen storage system by high-pressure torsion process. *Adv. Eng. Mater.* **2020**, *22*, 1900027.
39. Mohammadi, A.; Edalati, K.; Coimbrao, D.D.; Botta, W.J.; Noguchi, H. Influence of nanotwins on hydrogen embrittlement of TWIP (twinning-induced plasticity) steel processed by high-pressure torsion. *Mater. Sci. Eng. A* **2020**, *783*, 139273. [CrossRef]
40. Hongo, T.; Edalati, K.; Arita, M.; Matsuda, J.; Akiba, E.; Horita, Z. Significance of grain boundaries and stacking faults on hydrogen storage properties of Mg_2Ni intermetallics processed by high-pressure torsion. *Acta Mater.* **2015**, *92*, 46–54.
41. Mohammadi, A.; Edalati, P.; Arita, M.; Bae, J.W.; Kim, H.S.; Edalati, K. Microstructure and defect effects on strength and hydrogen embrittlement of high-entropy alloy CrMnFeCoNi processed by high-pressure torsion. *Mater. Sci. Eng. A* **2022**, *844*, 143179.
42. Krystian, M.; Setman, D.; Mingler, B.; Krexner, G.; Zehetbauer, M.J. Formation of superabundant vacancies in nano-Pd-H generated by high-pressure torsion. *Scr. Mater.* **2010**, *62*, 49–52. [CrossRef]
43. Čížek, J.; Janeček, M.; Vlasák, T.; Smola, B.; Melikhova, O.; Islamgaliev, R.K.; Dobatkin, S.V. The development of vacancies during severe plastic deformation. *Mater. Trans.* **2019**, *60*, 1533–1542. [CrossRef]
44. Hidalgo-Jiménez, J.; Akbay, T.; Ishihara, T.; Edalati, K. Understanding high photocatalytic activity of the TiO_2 high-pressure columbite phase by experiments and first-principles calculations. *J. Mater. Chem. A* **2023**, *11*, 23523–23535. [CrossRef]
45. Nguyen, T.T.; Sauvage, X.; Saito, K.; Guo, Q.; Edalati, K. Phase and sulfur vacancy engineering in cadmium sulfide for boosting hydrogen production from catalytic plastic waste photoconversion. *Chem. Eng. J.* **2025**, *504*, 158730. [CrossRef]
46. Pippan, R.; Scheriau, S.; Taylor, A.; Hafok, M.; Hohenwarter, A.; Bachmaier, A. Saturation of fragmentation during severe plastic deformation. *Annu. Rev. Mater. Res.* **2010**, *40*, 319–343. [CrossRef]
47. Renk, O.; Pippan, R. Saturation of grain refinement during severe plastic deformation of single phase materials: Reconsiderations, current status and open questions. *Mater. Trans.* **2019**, *60*, 1270–1282. [CrossRef]
48. Levitas, V.I. High-pressure phase transformations under severe plastic deformation by torsion in rotational anvils. *Mater. Trans.* **2019**, *60*, 1294–1301. [CrossRef]
49. Mazilkin, A.; Straumal, B.; Kilmametov, A.; Straumal, P.; Baretzky, B. Phase transformations induced by severe plastic deformation. *Mater. Trans.* **2019**, *60*, 1489–1499. [CrossRef]
50. Edalati, K. Superfunctional materials by ultra-severe plastic deformation. *Materials* **2023**, *16*, 587. [CrossRef] [PubMed]
51. Bachmaier, A.; Pippan, R. High-pressure torsion deformation induced phase transformations and formations: New material combinations and advanced properties. *Mater. Trans.* **2019**, *60*, 1256–1269. [CrossRef]
52. Edalati, K.; Matsuo, M.; Emami, H.; Itano, S.; Alhamidi, A.; Staykov, A.; Smith, D.J.; Orimo, S.; Akiba, E.; Horita, Z. Impact of severe plastic deformation on microstructure and hydrogen storage of titanium-iron-manganese intermetallics. *Scr. Mater.* **2016**, *124*, 108–111.
53. Edalati, K.; Kitabayashi, K.; Ikeda, Y.; Matsuda, J.; Li, H.W.; Tanaka, I.; Akiba, E.; Horita, Z. Bulk nanocrystalline gamma magnesium hydride with low dehydrogenation temperature stabilized by plastic straining via high-pressure torsion. *Scr. Mater.* **2018**, *157*, 54–57. [CrossRef]
54. Shundo, Y.; Nguyen, T.T.; Akrami, S.; Edalati, P.; Itagoe, Y.; Ishihara, T.; Arita, M.; Guo, Q.; Fuji, M.; Edalati, K. Oxygen vacancy-rich high-pressure rocksalt phase of zinc oxide for enhanced photocatalytic hydrogen evolution. *J. Colloid Interface Sci.* **2024**, *666*, 22–34. [PubMed]
55. Lopez-Gomez, E.I.; Edalati, K.; Antiqueira, F.J.; Coimbrao, D.D.; Zepon, G.; Leiva, D.R.; Ishikawa, T.T.; Cubero-Sesin, J.M.; Botta, W.J. Synthesis of nanostructured TiFe hydrogen storage material by mechanical alloying via high-pressure torsion. *Adv. Eng. Mater.* **2020**, *22*, 2000011.
56. Edalati, K.; Uehiro, R.; Ikeda, Y.; Li, H.W.; Emami, H.; Filinchuk, Y.; Arita, M.; Sauvage, X.; Tanaka, I.; Akiba, E.; et al. Design and synthesis of a magnesium alloy for room temperature hydrogen storage. *Acta Mater.* **2018**, *149*, 88–96. [CrossRef]
57. Segal, V.M. Review: Modes and processes of severe plastic deformation (SPD). *Materials* **2018**, *11*, 1175. [CrossRef]
58. Skrotzki, W. Deformation heterogeneities in equal channel angular pressing. *Mater. Trans.* **2019**, *60*, 1331–1343. [CrossRef]
59. Tsuji, N.; Saito, Y.; Lee, S.H.; Minamino, Y. ARB (accumulative roll-bonding) and other new techniques to produce bulk ultrafine grained materials. *Adv. Eng. Mater.* **2003**, *5*, 338–344.

60. Tsuji, N.; Gholizadeh, R.; Ueji, R.; Kamikawa, N.; Zhao, L.; Tian, Y.; Bai, Y.; Shibata, A. Formation mechanism of ultrafine grained microstructures: Various possibilities for fabricating bulk nanostructured metals and alloys. *Mater. Trans.* **2019**, *60*, 1518–1532. [CrossRef]
61. Miura, H.; Iwama, Y.; Kobayashi, M. Comparisons of microstructures and mechanical properties of heterogeneous nanostructure induced by heavy cold rolling and ultrafine-grained structure by multi-directional forging of Cu-Al alloy. *Mater. Trans.* **2019**, *60*, 1111–1115. [CrossRef]
62. Khodabackhshi, F.; Ekrt, O.; Abdi, M.; Gerlich, A.P.; Mottaghi, M.; Ebrahimi, R.; Nosko, M.; Wilde, G. Hydrogen storage behaviour of Mg/Ni layered nanostructure composite materials produced by accumulative fold-forging. *Int. J. Hydrogen Energy* **2022**, *47*, 1048–1062. [CrossRef]
63. Edalati, K.; Bachmaier, A.; Beloshenko, V.A.; Beygelzimer, Y.; Blank, V.D.; Botta, W.J.; Bryła, K.; Čížek, J.; Divinski, S.; Enikeev, N.A.; et al. Nanomaterials by severe plastic deformation: Review of historical developments and recent advances. *Mater. Res. Lett.* **2022**, *10*, 163–256. [CrossRef]
64. Edalati, K.; Ahmed, A.Q.; Akrami, S.; Ameyama, K.; Aptukov, V.; Asfandiyarov, R.N.; Ashida, M.; Astanin, V.; Bachmaier, A.; Beloshenko, V.; et al. Severe plastic deformation for producing superfunctional ultrafine-grained and heterostructured materials: An interdisciplinary review. *J. Alloys Compd.* **2024**, *1002*, 174667. [CrossRef]
65. Edalati, K.; Uehiro, R.; Fujiwara, K.; Ikeda, Y.; Li, H.W.; Sauvage, X.; Valiev, R.Z.; Akiba, E.; Tanaka, I.; Horita, Z. Ultra-severe plastic deformation: Evolution of microstructure, phase transformation and hardness in immiscible magnesium-based systems. *Mater. Sci. Eng. A* **2017**, *701*, 158–166. [CrossRef]
66. Howarth, R.W.; Jacobson, M.Z. How green is blue hydrogen? *Energy Sci. Eng.* **2021**, *9*, 1676–1687. [CrossRef]
67. Bauer, C.; Treyer, K.; Antonini, C.; Bergerson, J.; Gazzani, M.; Gencer, E.; Gibbins, J.; Mazzotti, M.; McCoy, S.T.; McKenna, R.; et al. On the climate impacts of blue hydrogen production. *Sustain. Energy Fuels* **2022**, *6*, 66–75.
68. Oliveira, A.M.; Beswick, R.R.; Yan, Y. A green hydrogen economy for a renewable energy society. *Curr. Opin. Chem. Eng.* **2021**, *33*, 100701. [CrossRef]
69. Wappler, M.; Unguder, D.; Lu, X.; Ohlmeyer, H.; Teschke, H.; Lueke, W. Building the green hydrogen market—Current state and outlook on green hydrogen demand and electrolyzer manufacturing. *Int. J. Hydrogen Energy* **2022**, *47*, 33551–33570. [CrossRef]
70. Kudo, A.; Miseki, Y. Heterogeneous photocatalyst materials for water splitting. *Chem. Soc. Rev.* **2009**, *38*, 253–278. [CrossRef]
71. Hisatomi, T.; Kubota, J.; Domen, K. Recent advances in semiconductors for photocatalytic and photoelectrochemical water splitting. *Chem. Soc. Rev.* **2014**, *43*, 7520–7535. [CrossRef]
72. Fu, W.; Zhang, Y.; Zhang, X.; Yang, H.; Xie, R.; Zhang, S.; Lv, Y.; Xiong, L. Progress in promising semiconductor materials for efficient photoelectrocatalytic hydrogen production. *Molecules* **2024**, *29*, 289. [CrossRef] [PubMed]
73. Yu, F.-Y.; Zhou, Y.-J.; Tan, H.-Q.; Li, Y.-G.; Kang, Z.-H. Versatile photoelectrocatalysis strategy raising up the green production of hydrogen peroxide. *Adv. Energy Mater.* **2023**, *13*, 2300119. [CrossRef]
74. Uekert, T.; Kuehnel, M.F.; Wakerley, D.W.; Reisner, E. Plastic waste as a feedstock for solar-driven H_2 generation. *Energy Environ. Sci.* **2018**, *11*, 2853–2857. [CrossRef]
75. Du, M.; Zhang, Y.; Kang, S.; Guo, X.; Ma, Y.; Xing, M.; Zhu, Y.; Chai, Y.; Qiu, B. Trash to treasure: Photoreforming of plastic waste into commodity chemicals and hydrogen over MoS_2-tipped CdS nanorods. *ACS Catal.* **2022**, *12*, 12823–12832.
76. Ouyang, L.; Jiang, J.; Chen, K.; Bai, L.; Wang, P.; Zhu, M. Hydrogen production via hydrolysis and alcoholysis of light metal-based materials: A review. *Nano-Micro Lett.* **2021**, *13*, 134. [CrossRef] [PubMed]
77. Liu, M.; Yao, Z.; Gu, J.; Li, C.; Huang, X.; Zhang, L.; Huang, Z.; Fan, M. Issues and opportunities facing hydrolytic hydrogen production materials. *Chem. Eng. J.* **2023**, *461*, 141918. [CrossRef]
78. Wang, H.Z.; Leung, D.Y.C.; Leung, M.K.H.; Ni, M. A review on hydrogen production using aluminum and aluminum alloys. *Renew. Sustain. Energy Rev.* **2009**, *13*, 845–853. [CrossRef]
79. Yoo, H.S.; Ryu, H.Y.; Cho, S.S.; Han, M.H.; Bae, K.S.; Lee, J.H. Effect of Si content on H production using Al-Si alloy powders. *Int. J. Hydrogen Energy* **2011**, *36*, 15111–15118. [CrossRef]
80. Soler, L.; Macanas, J.; Munoz, M.; Casado, J. Aluminum and aluminum alloys as sources of hydrogen for fuel cell application. *J. Power Sources* **2007**, *169*, 144–149. [CrossRef]
81. Zhang, F.; Yonemoto, R.; Arita, M.; Horita, Z. Hydrogen generation from pure water using Al-Sn powders consolidated through high-pressure torsion. *J. Mater. Res.* **2016**, *31*, 775–782. [CrossRef]
82. Zhang, F.; Edalati, K.; Arita, M.; Horita, Z. Fast hydrolysis and hydrogen generation on Al-Bi alloys and Al-Bi-C composites synthesized by high-pressure torsion. *Int. J. Hydrogen Energy* **2017**, *42*, 29121–29130. [CrossRef]
83. Zhang, F.; Edalati, K.; Arita, M.; Horita, Z. Hydrolytic hydrogen production on Al-Sn-Zn alloys processed by high-pressure torsion. *Materials* **2018**, *11*, 1209.
84. Masa, J.; Andronescu, C.; Schuhmann, W. Electrocatalysis as the nexus for sustainable renewable energy: The Gordian knot of activity, stability, and selectivity. *Angew. Chem.* **2020**, *59*, 15298–15312. [CrossRef] [PubMed]

85. Zhai, W.; Ma, Y.; Chen, D.; Ho, J.C.; Dai, Z.; Qu, Y. Recent progress on the long-term stability of hydrogen evolution reaction electrocatalysts. *InfoMat* **2022**, *4*, e12357.
86. Edalati, K.; Wang, Q.; Eguchi, H.; Razavi-Khosroshahi, H.; Emami, H.; Yamauchi, M.; Fuji, M.; Horita, Z. Impact of TiO_2-II phase stabilized in anatase matrix by high-pressure torsion on electrocatalytic hydrogen production. *Mater. Res. Lett.* **2019**, *7*, 334–339. [CrossRef]
87. Wu, K.; Meng, Y.; Xu, J.; Edalati, K.; Shao, H.; Li, W.; Lin, H.J. Novel Fe-based nanoglass: An efficient noble-metal-free electrocatalyst for alkaline hydrogen evolution reaction. *Scr. Mater.* **2020**, *188*, 135–139.
88. Chu, F.; Wu, K.; Meng, Y.; Edalati, K.; Lin, H.J. Effect of high-pressure torsion on the hydrogen evolution performances of a melt-spun amorphous $Fe_{73.5}Si_{13.5}B_9Cu_1Nb_3$ alloy. *Int. J. Hydrogen Energy* **2021**, *46*, 25029–25038.
89. Chu, F.; Han, B.; Edalati, K.; Ma, J.; Meng, Y.; Wang, C.; Yang, F.; Zhang, P.; Lin, H.J. Severe plastic deformed Pd-based metallic glass for superior hydrogen evolution in both acidic and alkaline media. *Scr. Mater.* **2021**, *204*, 114145. [CrossRef]
90. Chu, F.; Jian, X.; Edalati, K.; Yan, Y.; Ke, H.; Zhang, P.; Lin, H.J. Nanoscale heterogeneous FeB metallic glass as highly active and stable catalyst for hydrogen evolution. *J. Alloys Compd.* **2023**, *960*, 170964. [CrossRef]
91. Jian, X.; Li, J.; He, L.; Li, H.W.; Zhang, M.; Zhang, P.; Lin, H.J. Severe plastic deformation for advanced electrocatalysts for electrocatalytic hydrogen production. *Mater. Trans.* **2023**, *64*, 1515–1525. [CrossRef]
92. Fujishima, A.; Honda, K. Electrochemical photolysis of water at a semiconductor electrode. *Nature* **1972**, *238*, 37–38. [CrossRef]
93. Tao, X.; Zhao, Y.; Wang, S.; Li, C.; Li, R. Recent advances and perspectives for solar-driven water splitting using particulate photocatalysts. *Chem. Soc. Rev.* **2022**, *51*, 3561–3608. [CrossRef]
94. Samanta, B.; Morales-García, Á.; Illas, F.; Goga, N.; Anta, J.A.; Calero, S.; Bieberle-Hütter, A.; Libisch, F.; Muñoz-García, A.B.; Pavone, M.; et al. Challenges of modeling nanostructured materials for photocatalytic water splitting. *Chem. Soc. Rev.* **2022**, *51*, 3794–3818. [CrossRef]
95. Mohamadpour, F.; Amani, A.M. Photocatalytic systems: Reactions, mechanism, and applications. *RSC Adv.* **2024**, *14*, 20609–20645. [CrossRef]
96. Edalati, K. Review on recent advancement in severe plastic deformation of oxides by high-pressure torsion (HPT). *Adv. Eng. Mater.* **2019**, *21*, 1800272.
97. Akrami, S.; Edalati, P.; Fuji, M.; Edalati, K. High-pressure torsion for highly-strained and high-entropy photocatalysts. *KONA Powder Part. J.* **2024**, *41*, 123–139.
98. Sena, H.; Fuji, M. Band gap engineering of semiconductors and ceramics by severe plastic deformation for solar energy harvesting. *Mater. Trans.* **2023**, *64*, 1497–1503. [CrossRef]
99. Razavi-Khosroshahi, H.; Edalati, K.; Hirayama, M.; Emami, H.; Arita, M.; Yamauchi, M.; Hagiwara, H.; Ida, S.; Ishihara, T.; Akiba, E.; et al. Visible-light-driven photocatalytic hydrogen generation on TiO_2-II stabilized by high-pressure torsion. *ACS Catal.* **2016**, *6*, 5103–5107. [CrossRef]
100. Wang, Q.; Edalati, K.; Koganemaru, Y.; Nakamura, S.; Watanabe, M.; Ishihara, T.; Horita, Z. Photocatalytic hydrogen generation on low-bandgap black zirconia (ZrO_2) produced by high-pressure torsion. *J. Mater. Chem. A* **2020**, *8*, 3643–3650. [CrossRef]
101. Nguyen, T.T.; Edalati, K. Efficient photocatalytic hydrogen production on defective and strained black bismuth (III) oxide. *Int. J. Hydrogen Energy* **2024**, *96*, 841–846. [CrossRef]
102. Hidalgo-Jimenez, J.; Wang, Q.; Edalati, K.; Cubero-Sesin, J.; Razavi-Khosroshahi, H.; Ikoma, Y.; Gutierrez-Fallas, D.; Dittel-Meza, F.A.; Rodriguez-Rufino, J.C.; Fuji, M.; et al. High-pressure torsion of TiO_2-ZnO composites: Phase transformations, vacancy formation and changes in optical and photocatalytic properties. *Int. J. Plast.* **2020**, *124*, 170–185. [CrossRef]
103. Nguyen, T.T.; Edalati, K. High-pressure phase and dual sulfur-oxygen vacancy induction in CdS-TiO_2 heterojunctions for multifunctional photocatalytic applications. *Acta Mater.* **2025**, *301*, 121555. [CrossRef]
104. Edalati, P.; Wang, Q.; Razavi-Khosroshahi, H.; Fuji, M.; Ishihara, T.; Edalati, K. Photocatalytic hydrogen evolution on a high-entropy oxide. *J. Mater. Chem. A* **2020**, *8*, 3814–3821. [CrossRef]
105. Edalati, P.; Shen, X.F.; Watanabe, M.; Ishihara, T.; Arita, M.; Fuji, M.; Edalati, K. High-entropy oxynitride as low-bandgap and stable photocatalyst for hydrogen production. *J. Mater. Chem. A* **2021**, *9*, 15076–15086. [CrossRef]
106. Chen, F.; Ma, T.; Zhang, T.; Zhang, Y.; Huang, H. Atomic-level charge separation strategies in semiconductor-based photocatalysts. *Adv. Mater.* **2021**, *33*, 2005256.
107. Akrami, S.; Edalati, P.; Shundo, Y.; Watanabe, M.; Ishihara, T.; Fuji, M.; Edalati, K. Significant CO_2 photoreduction on a high-entropy oxynitride. *Chem. Eng. J.* **2022**, *449*, 137800. [CrossRef]
108. Hanaor, D.A.H.; Sorrell, C.C. Review of the anatase to rutile phase transformation. *J. Mater. Sci.* **2011**, *46*, 855–874. [CrossRef]
109. Ong, C.B.; Ng, L.Y.; Mohammad, A.W. A review of ZnO nanoparticles as solar photocatalysts: Synthesis, mechanisms and applications. *Renew. Sustain. Energy Rev.* **2018**, *81*, 536–551. [CrossRef]
110. Oberdorfer, B.; Lorenzoni, B.; Unger, K.; Sprengel, W.; Zehetbauer, M.; Pippan, R.; Würschum, R. Absolute concentration of free volume-type defects in ultrafine-grained Fe prepared by high-pressure torsion. *Scr. Mater.* **2010**, *63*, 452–455. [CrossRef]

111. Chen, X.; Liu, L.; Yu, P.Y.; Mao, S.S. Increasing solar absorption for photocatalysis with black hydrogenated titanium dioxide nanocrystals. *Science* **2011**, *331*, 746–750. [CrossRef]
112. Cui, H.; Zhu, G.; Xie, Y.; Zhao, W.; Yang, C.; Lin, T.; Gu, H.; Huang, F. Black nanostructured Nb_2O_5 with improved solar absorption and enhanced photoelectrochemical water splitting. *J. Mater. Chem. A* **2015**, *3*, 11830–11837. [CrossRef]
113. Katai, M.; Edalati, P.; Hidalgo-Jimenez, J.; Shundo, Y.; Akbay, T.; Ishihara, T.; Arita, M.; Fuji, M.; Edalati, K. Black brookite rich in oxygen vacancies as an active photocatalyst for CO_2 conversion: Experiments and first-principles calculations. *J. Photochem. Photobiol. A* **2024**, *449*, 115409. [CrossRef]
114. Edalati, K.; Fujiwara, K.; Takechi, S.; Wang, Q.; Arita, M.; Watanabe, M.; Sauvage, X.; Ishihara, T.; Horita, Z. Improved photocatalytic hydrogen evolution on tantalate perovskites $CsTaO_3$ and $LiTaO_3$ by strain-induced vacancies. *ACS Appl. Energy Mater.* **2020**, *3*, 1710–1718. [CrossRef]
115. Edalati, K.; Uehiro, R.; Takechi, S.; Wang, Q.; Arita, M.; Watanabe, M.; Ishihara, T.; Horita, Z. Enhanced photocatalytic hydrogen production on GaN-ZnO oxynitride by introduction of strain-induced nitrogen vacancy complexes. *Acta Mater.* **2020**, *185*, 149–156. [CrossRef]
116. Xu, Q.; Wageh, S.; Al-Ghamdi, A.A.; Li, X. Design principle of S-scheme heterojunction photocatalyst. *J. Mater. Sci. Technol.* **2022**, *124*, 171–173. [CrossRef]
117. Wang, C.; Zhao, Y.; Cheng, C.; Li, Q.; Guo, C.; Hu, Y. S-scheme heterojunction photocatalysts: Mechanism, challenges and opportunities. *Coord. Chem. Rev.* **2024**, *521*, 216177.
118. Yang, H. A short review on heterojunction photocatalysts: Carrier transfer behavior and photocatalytic mechanisms. *Mater. Res. Bull.* **2021**, *142*, 111406. [CrossRef]
119. Zu, D.; Wei, H.; Lin, Z.; Bai, X.; Ivan, M.N.A.S.; Tsang, Y.H.; Huang, H. The role of point defects in heterojunction photocatalysts: Perspectives and outlooks. *Adv. Funct. Mater.* **2024**, *48*, 2408213.
120. Hai, H.T.N.; Hidalgo-Jiménez, J.; Edalati, K. Boosting hydrogen and methane formation on a high-entropy photocatalyst by integrating atomic d^0/d^{10} electronic junctions and microscopic P/N heterojunctions. *Int. J. Hydrogen Energy* **2025**, *162*, 150762. [CrossRef]
121. Edalati, P.; Itagoe, Y.; Ishihara, H.; Ishihara, T.; Emami, H.; Arita, M.; Fuji, M.; Edalati, K. Visible-light photocatalytic oxygen production on a high-entropy oxide with multiple-heterojunction introduction. *J. Photochem. Photobiol. A* **2022**, *433*, 114167.
122. Yeh, J.W.; Chen, S.K.; Lin, S.J.; Gan, J.Y.; Chin, T.S.; Shun, T.T.; Tsau, C.H.; Chang, S.Y. Nanostructured high-entropy alloys with multiple principal elements: Novel alloy design concepts and outcomes. *Adv. Eng. Mater.* **2004**, *6*, 299–303. [CrossRef]
123. Cantor, B.; Chang, I.; Knight, P.; Vincent, A. Microstructural development in equiatomic multicomponent alloys. *Mater. Sci. Eng. A* **2004**, *375*, 213–218. [CrossRef]
124. Oses, C.; Toher, C.; Curtarolo, S. High-entropy ceramics. *Nat. Rev. Mater.* **2020**, *5*, 295–309. [CrossRef]
125. Akrami, S.; Edalati, P.; Fuji, M.; Edalati, K. High-entropy ceramics: Review of principles, production and applications. *Mater. Sci. Eng. R* **2021**, *146*, 100644. [CrossRef]
126. Edalati, P.; Fuji, M.; Edalati, K. Superfunctional high-entropy alloys and ceramics by severe plastic deformation. *Rare Met.* **2023**, *42*, 3246–3268. [CrossRef]
127. Hidalgo-Jiménez, J.; Akbay, T.; Sauvage, X.; van Eijck, L.; Huot, J.; Ishihara, T.; Edalati, K. Hybrid d^0 and d^{10} electronic configurations promote photocatalytic activity of high-entropy oxides for CO_2 conversion and water splitting. *J. Mater. Chem. A* **2024**, *12*, 31589–31602. [CrossRef]
128. Hidalgo-Jiménez, J.; Akbay, T.; Sauvage, X.; Ishihara, T.; Edalati, K. Mixed atomic-scale electronic configuration as a strategy to avoid cocatalyst utilization in photocatalysis by high-entropy oxides. *Acta Mater.* **2025**, *283*, 120559. [CrossRef]
129. Hidalgo-Jiménez, J.; Akbay, T.; Watanabe, M.; Saito, K.; Guo, Q.; Ishihara, T.; Edalati, K. Entropy-stabilized oxides with d^{10} and s^0p^0 cations as heterostructured photocatalysts with high work function: Experiments and first-principles calculations. *J. Energy Chem.* **2025**, *111*, 954–968. [CrossRef]
130. Hidalgo-Jiménez, J.; Akbay, T.; Ishihara, T.; Edalati, K. Active high-entropy photocatalyst designed by incorporating alkali metals to achieve $d^0 + d^{10} + s^0$ cationic configurations and wide electronegativity mismatch. *Acta Mater.* **2026**, *32*, 121632. [CrossRef]
131. Hidalgo-Jiménez, J.; Akbay, T.; Ishihara, T.; Edalati, K. Investigation of a high-entropy oxide photocatalyst for hydrogen generation by first-principles calculations coupled with experiments: Significance of electronegativity. *Scr. Mater.* **2024**, *250*, 116205. [CrossRef]
132. Hai, H.T.N.; Arita, M.; Edalati, K. High-entropy perovskites as new photocatalysts for cocatalyst-free water splitting. *Appl. Catal. B* **2026**, *383*, 126081.
133. Tehrani, Z.P.; Fromme, T.; Reichenberger, S.; Gökcee, B.; Ishihara, T.; Lippert, T.; Edalati, K. Laser fragmentation of high-entropy oxide for enhanced photocatalytic carbon dioxide (CO_2) conversion and hydrogen (H_2) production. *Adv. Powder Technol.* **2024**, *35*, 104448. [CrossRef]
134. Wang, J.; Wang, Z.; Zhang, J.; Mamatkulov, S.; Dai, K.; Ruzimuradov, O.; Low, J. Two-dimensional high-entropy selenides for boosting visible-light-driven photocatalytic performance. *ACS Nano* **2024**, *18*, 20740–20750. [CrossRef] [PubMed]

135. Ling, H.; Sun, H.; Lu, L.; Zhang, J.; Liao, L.; Wang, J.; Zhang, X.; Lan, Y.; Li, R.; Lu, W.; et al. Sustainable photocatalytic hydrogen peroxide production over octonary high-entropy oxide. *Nat. Commun.* **2024**, *15*, 9505. [CrossRef] [PubMed]
136. Bai, W.; Chang, F.; Li, K.; Kou, Y.; Tian, W. High-entropy materials for photocatalysis: A mini review. *Catalysts* **2025**, *15*, 1152. [CrossRef]
137. Monfort, O.; Pop, L.-C.; Sfaelou, S.; Plecenik, T.; Roch, T.; Dracopoulos, V.; Stathatos, E.; Plesch, G.; Lianos, P. Photoelectrocatalytic hydrogen production by water splitting using $BiVO_4$ photoanodes. *Chem. Eng. J.* **2016**, *286*, 91–97. [CrossRef]
138. Bora, L.V.; Bora, N.V. Photoelectrocatalytic water splitting for efficient hydrogen production: A strategic review. *Fuel* **2025**, *381*, 133642. [CrossRef]
139. Nguyen, T.T.; Arita, M.; Saeki, R.; Edalati, K. High-entropy oxide Ti-Zr-Hf-Nb-Ta-O as photoanode for photoelectrocatalytic hydrogen generation. *Scr. Mater.* **2025**, *264*, 116698.
140. Shelake, S.P.; Sutar, D.N.; Abraham, B.M.; Banerjee, T.; Sainath, A.V.S.; Pal, U. Emerging photoreforming process to hydrogen production: A future energy. *Adv. Funct. Mater.* **2024**, *34*, 2403795. [CrossRef]
141. Li, H.; Huang, Y.; Zhang, Y.; Li, H.; Shen, C.; Xia, D.; Zheng, Y. Plastic photoreforming: Catalytic production of hydrogen and valuable chemicals. *Green Chem.* **2025**, *27*, 12050–12069. [CrossRef]
142. Nagakawa, H.; Nagata, M. Photoreforming of organic waste into hydrogen using a thermally radiative CdO_x/CdS/SiC photocatalyst. *ACS Appl. Mater. Interfaces* **2021**, *13*, 47511–47519. [CrossRef] [PubMed]
143. Han, M.; Zhu, S.; Xia, C.; Yang, B. Photocatalytic upcycling of poly(ethylene terephthalate) plastic to high-value chemicals. *Appl. Catal. B* **2022**, *316*, 120764.
144. Lai, Y.H.; Yeh, P.W.; Jhong, M.J.; Chuang, P.C. Solar-driven hydrogen evolution in alkaline seawater over earth-abundant g-C_3N_4/$CuFeO_2$ heterojunction photocatalyst using microplastic as a feedstock. *Chem. Eng. J.* **2023**, *475*, 146413.
145. Peng, G.; Qi, X.; Qu, Q.; Shao, X.; Song, L.; Du, P.; Xiong, J. Photocatalytic degradation of PET microfibers and hydrogen evolution by Ni_5P_4/TiO_2/C NFs. *Catal. Sci. Technol.* **2023**, *13*, 5868–5879.
146. Wenbin, Q.; Qi, X.; Peng, G.; Wang, M.; Song, L.; Du, P.; Xiong, J. An efficient and recyclable Ni_2P-Co_2P/ZrO_2/C nanofiber photocatalyst for the conversion of plastic waste into H_2 and valuable chemicals. *J. Mater. Chem. C* **2023**, *11*, 14359–14370.
147. Jiang, D.; Yuan, H.; Liu, Z.; Chen, Y.; Li, Y.; Zhang, X.; Xue, G.; Liu, H.; Liu, X.; Zhao, L.; et al. Defect-anchored single-atom-layer Pt clusters on TiO_{2-x}/Ti for efficient hydrogen evolution via photothermal reforming plastics. *Appl. Catal. B* **2023**, *339*, 123081.
148. Yuting, J.; Zhang, H.; Hong, L.; Shao, J.; Zhang, B.; Yu, J.; Chu, S. An integrated plasma-photocatalytic system for upcycling of polyolefin plastics. *ChemSusChem* **2023**, *16*, e202300106.
149. Nguyen, T.T.; Edalati, K. Efficient photoreforming of plastic waste using a high-entropy oxide catalyst. *J. Catal.* **2024**, *440*, 115808. [CrossRef]
150. Hai, H.T.N.; Nguyen, T.T.; Nishibori, M.; Ishihara, T.; Edalati, K. Photoreforming of plastic waste into valuable products and hydrogen using a high-entropy oxynitride with distorted atomic-scale structure. *Appl. Catal. B* **2025**, *365*, 124968. [CrossRef]
151. Nguyen, T.T.; Edalati, K. Impact of high-pressure columbite phase of titanium dioxide (TiO_2) on catalytic photoconversion of plastic waste and simultaneous hydrogen (H_2) production. *J. Alloys Compd.* **2024**, *1008*, 176722.
152. Nguyen, T.T.; Edalati, K. Impact of high-pressure torsion on hydrogen production from photodegradation of polypropylene plastic wastes. *Int. J. Hydrogen Energy* **2024**, *81*, 411–417. [CrossRef]
153. Nguyen, T.T.; Nguyen, T.V.; Takahara, A.; Edalati, K. Solar light irradiation pre-treatment followed by photoreforming for simultaneous polypropylene (PP) plastic degradation and hydrogen production. *J. Environ. Chem. Eng.* **2025**, *13*, 116944. [CrossRef]
154. Skripnyuk, V.M.; Rabkin, E.; Estrin, Y.; Lapovok, R. The effect of ball milling and equal channel angular pressing on the hydrogen absorption/desorption properties of Mg-4.95 wt% Zn-0.71 wt% Zr (ZK60) alloy. *Acta Mater.* **2004**, *52*, 405–414. [CrossRef]
155. Skripnyuk, V.; Buchman, E.; Rabkin, E.; Estrin, M.; Popov, S.; Jorgensen, S. The effect of equal channel angular pressing on hydrogen storage properties of a eutectic Mg-Ni alloy. *J. Alloys Compd.* **2007**, *436*, 99–106. [CrossRef]
156. Asselli, A.A.C.; Leiva, D.R.; Huot, J.; Kawasaki, M.; Langdon, T.G.; Botta, W.J. Effects of equal-channel angular pressing and accumulative roll-bonding on hydrogen storage properties of a commercial ZK60 magnesium alloy. *Int. J. Hydrogen Energy* **2015**, *40*, 16971–16976. [CrossRef]
157. Jorge, A.M., Jr.; Prokofiev, E.; Martins Triques, M.R.; Roche, V.; Botta, W.J.; Kiminami, C.S.; Raab, G.I.; Valiev, R.Z.; Langdon, T.G. Effect of cold rolling on the structure and hydrogen properties of AZ91 and AM60D magnesium alloys processed by ECAP. *Int. J. Hydrogen Energy* **2017**, *42*, 21822–21831. [CrossRef]
158. Skryabina, N.; Aptukov, V.; Romanov, P.; Fruchart, D.; de Rango, P.; Girard, G.; Grandini, C.; Sandim, H.; Huot, J.; Lang, J.; et al. Microstructure optimization of Mg-alloys by the ECAP process including numerical simulation, SPD treatments, characterization, and hydrogen sorption properties. *Molecules* **2019**, *24*, 89. [CrossRef]
159. Mori, R.; Miyamura, H.; Kikuchi, S.; Tanaka, K.; Takeichi, N.; Tanaka, H.; Kuriyama, N.; Ueda, T.T.; Tsukahara, M. Hydrogenation characteristics of Mg based alloy prepared by super lamination technique. *Mater. Sci. Forum* **2007**, *561–565*, 1609–1612. [CrossRef]

160. Vincent, S.D.; Lang, J.; Huot, J. Addition of catalysts to magnesium hydride by means of cold rolling. *J. Alloys Compd.* **2012**, *512*, 290–295. [CrossRef]
161. Huot, J.; Amira, S.; Lang, J.; Skryabina, N.; Fruchart, D. Improvement of hydrogen storage properties of magnesium alloys by cold rolling and forging. *IOP Conf. Ser. Mater. Sci. Eng.* **2014**, *63*, 012114. [CrossRef]
162. Márquez, J.J.; Leiva, D.R.; Floriano, R.; Silva, W.B.; Ishikawa, T.T.; Kiminami, C.S.; Botta, W.J. Hydrogen storage in MgH_2-$LaNi_5$ composites prepared by cold rolling under inert atmosphere. *Int. J. Hydrogen Energy* **2018**, *43*, 13348–13355. [CrossRef]
163. Floriano, R.; Leiva, D.R.; Melo, G.C.; Ishikawa, T.T.; Huot, J.; Kaufman, M.; Figueroa, S.J.A.; Mendoza-Zélis, L.A.; Damonte, L.C.; Botta, W.J. Low temperature rolling of AZ91 alloy for hydrogen storage. *Int. J. Hydrogen Energy* **2017**, *42*, 29394–29405. [CrossRef]
164. de Rango, P.; Fruchart, D.; Aptukov, V.; Skryabina, N. Fast forging: A new SPD method to synthesize Mg-based alloys for hydrogen storage. *Int. J. Hydrogen Energy* **2020**, *45*, 7912–7916. [CrossRef]
165. Skryabina, N.; Aptukov, V.N.; de Rango, P.; Fruchart, D. Effect of temperature on fast forging process of Mg-Ni samples for fast formation of Mg_2Ni for hydrogen storage. *Int. J. Hydrogen Energy* **2020**, *45*, 3008–3015. [CrossRef]
166. de Rango, P.; Wen, J.; Skryabina, N.; Laversenne, L.; Fruchart, D.; Borges, M. Hydrogen storage properties of Mg-Ni alloys processed by fast forging. *Energies* **2020**, *13*, 3509. [CrossRef]
167. Wen, J.; de Rango, P.; Allain, N.; Laversenne, L.; Grosdidier, T. Improving hydrogen storage performance of Mg-based alloy through microstructure optimization. *J. Power Sources* **2020**, *480*, 228823. [CrossRef]
168. Wen, J.; de Rango, P.; Allain, N.; Novelli, M.; Grosdidier, T.; Laversenne, L. In situ observation and kinetic modeling of the fundamental mechanisms underlying hydrogen sorption in forged Mg–Mg_2Ni composites. *Int. J. Hydrogen Energy* **2024**, *94*, 1160–1173. [CrossRef]
169. Kusadome, Y.; Ikeda, K.; Nakamori, Y.; Orimo, S.; Horita, Z. Hydrogen storage capability of $MgNi_2$ processed by high pressure torsion. *Scr. Mater.* **2007**, *57*, 751–753. [CrossRef]
170. Révész, Á.; Kánya, Z.; Verebélyi, T.; Szabó, P.J.; Zhilyaev, A.P.; Spassov, T. The effect of high-pressure torsion on the microstructure and hydrogen absorption kinetics of ball-milled $Mg_{70}Ni_{30}$. *J. Alloys Compd.* **2010**, *504*, 83–88. [CrossRef]
171. Leiva, D.R.; Jorge, A.M.; Ishikawa, T.T.; Huot, J.; Fruchart, D.; Miraglia, S.; Kiminami, C.S.; Botta, W.J. Nanoscale grain refinement and H-sorption properties of MgH_2 processed by high-pressure torsion and other mechanical routes. *Adv. Eng. Mater.* **2010**, *12*, 786–792. [CrossRef]
172. Zou, J.X.; Perez-Brokate, C.F.; Arruffat, R.; Bolle, B.; Fundenberger, J.J.; Zeng, X.Q.; Grosdidier, T.; Ding, W.J. Nanostructure bulk Mg + MgO composite synthesized through arc-plasma evaporation and high pressure torsion for H-storage application. *Mater. Sci. Eng. B* **2014**, *183*, 1–5.
173. Grill, A.; Horky, J.; Panigrahi, A.; Krexner, G.; Zehetbauer, M. Long-term hydrogen storage in Mg and ZK60 after severe plastic deformation. *Int. J. Hydrogen Energy* **2015**, *40*, 17144–17152. [CrossRef]
174. Panda, S.; Fundenberger, J.J.; Zhao, Y.; Zou, J.; Toth, L.S.; Grosdidier, T. Effect of initial powder type on the hydrogen storage properties of high-pressure torsion consolidated Mg. *Int. J. Hydrogen Energy* **2017**, *42*, 22438–22448. [CrossRef]
175. Grosdidier, T.; Fundenberger, J.J.; Zou, J.X.; Pan, Y.C.; Zeng, X.Q. Nanostructured Mg based hydrogen storage bulk materials prepared by high pressure torsion consolidation of arc plasma evaporated ultrafine powders. *Int. J. Hydrogen Energy* **2015**, *40*, 16985–16991. [CrossRef]
176. Panda, S.; Toth, L.S.; Zou, J.; Grosdidier, T. Effect of strain heterogeneities on microstructure, texture, hardness, and H-activation of high-pressure torsion Mg consolidated from different powders. *Materials* **2018**, *11*, 1335. [PubMed]
177. Gajdics, M.; Calizzi, M.; Pasquini, L.; Schafler, E.; Révész, Á. Characterization of a nanocrystalline Mg-Ni alloy processed by high-pressure torsion during hydrogenation and dehydrogenation. *Int. J. Hydrogen Energy* **2016**, *41*, 9803–9809. [CrossRef]
178. Edalati, K.; Novelli, M.; Itano, S.; Li, H.W.; Akiba, E.; Horita, Z.; Grosdidier, T. Effect of gradient-structure versus uniform nanostructure on hydrogen storage of Ti-V-Cr alloys: Investigation using ultrasonic SMAT and HPT processes. *J. Alloys Compd.* **2017**, *737*, 337–346.
179. Novelli, M.; Edalati, K.; Itano, S.; Li, H.W.; Akiba, E.; Horita, Z.; Grosdidier, T. Microstructural details of hydrogen diffusion and storage in Ti-V-Cr alloys activated through surface and bulk severe plastic deformation. *Int. J. Hydrogen Energy* **2020**, *45*, 5326–5336.
180. Edalati, K.; Matsuda, J.; Arita, M.; Daio, T.; Akiba, E.; Horita, Z. Mechanism of activation of TiFe intermetallics for hydrogen storage by severe plastic deformation using high-pressure torsion. *Appl. Phys. Lett.* **2013**, *103*, 143902.
181. Edalati, K.; Matsuda, J.; Yanagida, A.; Akiba, E.; Horita, Z. Activation of TiFe for hydrogen storage by plastic deformation using groove rolling and high-pressure torsion: Similarities and differences. *Int. J. Hydrogen Energy* **2014**, *39*, 15589–15594.
182. Révész, Á.; Gajdics, M.; Schafler, E.; Calizzi, M.; Pasquini, L. Dehydrogenation-hydrogenation characteristics of nanocrystalline Mg_2Ni powders compacted by high-pressure torsion. *J. Alloys Compd.* **2017**, *702*, 84–91. [CrossRef]
183. Révész, Á.; Kis-Tóth, Á.; Varga, L.K.; Schafler, E.; Bakonyi, I.; Spassov, T. Hydrogen storage of melt-spun amorphous $Mg_{65}Ni_{20}Cu_5Y_{10}$ alloy deformed by high-pressure torsion. *Int. J. Hydrogen Energy* **2012**, *37*, 5769–5776. [CrossRef]

184. Xu, C.; Lin, H.; Edalati, K.; Li, W.; Li, L.; Zhu, Y. Superior hydrogenation properties in a $Mg_{65}Ce_{20}Ni_{10}Cu_5$ nanoglass processed by melt-spinning followed by high-pressure torsion. *Scr. Mater.* **2018**, *152*, 137–140. [CrossRef]
185. Wang, K.; Edalati, K.; Lu, Y.; Huang, L.; Wang, H.; Lin, H.J. Tailoring structural order and hydrogenation properties of a Mg-based amorphous alloy by high-pressure torsion. *J. Alloys Compd.* **2025**, *1049*, 185393. [CrossRef]
186. Edalati, P.; Floriano, R.; Mohammadi, A.; Li, Y.; Zepon, G.; Li, H.W.; Edalati, K. Reversible room temperature hydrogen storage in high-entropy alloy TiZrCrMnFeNi. *Scr. Mater.* **2020**, *178*, 387–390. [CrossRef]
187. Hidalgo-Jiménez, J.; Cubero-Sesin, J.M.; Edalati, K.; Khajavi, S.; Huot, J. Effect of high-pressure torsion on first hydrogenation of Laves phase $Ti_{0.5}Zr_{0.5}(Mn_{1-x}Fe_x)Cr_1$ (x = 0, 0.2 and 0.4) high entropy alloy. *J. Alloys Compd.* **2023**, *969*, 172243. [CrossRef]
188. Ueda, T.; Yoshida, S.; Dangwal, S.; Gondek, Ł.; Fukami, K.; Kučerová, L.; Saksl, K.; Edalati, K.; Tsuji, N. Effect of lattice defects on hydrogen storage properties of HfNbTiZr medium entropy alloy. *Int. J. Hydrogen Energy* **2025**, *155*, 150292. [CrossRef]
189. Gajdics, M.; Spassov, T.; Kis, V.K.; Schafler, E.; Révész, Á. Microstructural and morphological investigations on Mg-Nb_2O_5-CNT nanocomposites processed by high-pressure torsion for hydrogen storage applications. *Int. J. Hydrogen Energy* **2020**, *45*, 7917–7928. [CrossRef]
190. Leiva, D.R.; Jorge, A.M., Jr.; Ishikawa, T.T.; Botta, W.J. Hydrogen storage in Mg and Mg-based alloys and composites processed by severe plastic deformation. *Mater. Trans.* **2019**, *60*, 1561–1570. [CrossRef]
191. Osorio-García, M.; Suárez-Alcántara, K.; Todaka, Y.; Tejeda-Ochoa, A.; Herrera-Ramírez, M.; Hernández-Silva, O.; Cruz-Gandarilla, F.; Cabañas-Moreno, J.G. Low-temperature hydrogenation of Mg-Ni-Nb_2O_5 alloy processed by high-pressure torsion. *J. Alloys Compd.* **2021**, *878*, 160309. [CrossRef]
192. Emami, H.; Edalati, K.; Staykov, A.; Hongo, T.; Iwaoka, H.; Horita, Z.; Akiba, E. Solid-state reactions and hydrogen storage in magnesium mixed with various elements by high-pressure torsion: Experiments and first-principles calculations. *RSC Adv.* **2016**, *6*, 11665–11674.
193. Edalati, K.; Emami, H.; Staykov, A.; Smith, D.J.; Akiba, E.; Horita, Z. Formation of metastable phases in magnesium-titanium system by high-pressure torsion and their hydrogen storage performance. *Acta Mater.* **2015**, *50*, 150–156.
194. Edalati, K.; Emami, H.; Ikeda, Y.; Iwaoka, H.; Tanaka, I.; Akiba, E.; Horita, Z. New nanostructured phases with reversible hydrogen storage capability in immiscible magnesium-zirconium system produced by high-pressure torsion. *Acta Mater.* **2016**, *108*, 293–303.
195. Fujiwara, K.; Uehiro, R.; Edalati, K.; Li, H.W.; Floriano, R.; Akiba, E.; Horita, Z. New Mg-V-Cr BCC alloys synthesized by high-pressure torsion and ball milling. *Mater. Trans.* **2018**, *59*, 741–746.
196. De Marco, M.O.; Li, Y.; Li, H.W.; Edalati, K.; Floriano, R. Mechanical synthesis and hydrogen storage characterization of MgVCr and MgVTiCrFe high-entropy alloy. *Adv. Eng. Mater.* **2020**, *22*, 1901079.
197. Edalati, K.; Yamamoto, A.; Horita, Z.; Ishihara, T. High-pressure torsion of pure magnesium: Evolution of mechanical properties, microstructures and hydrogen storage capacity with equivalent strain. *Scr. Mater.* **2011**, *64*, 880–883. [CrossRef]
198. Edalati, K.; Matsuda, J.; Iwaoka, H.; Toh, S.; Akiba, E.; Horita, Z. High-pressure torsion of TiFe intermetallics for activation of hydrogen storage at room temperature with heterogeneous nanostructure. *Int. J. Hydrogen Energy* **2013**, *38*, 4622–4627.
199. Edalati, K.; Shao, H.; Emami, H.; Iwaoka, H.; Horita, Z.; Akiba, E. Activation of titanium-vanadium alloy for hydrogen storage by introduction of nanograins and edge dislocations using high-pressure torsion. *Int. J. Hydrogen Energy* **2016**, *41*, 8917–8924.
200. Edalati, K.; Toh, S.; Watanabe, M.; Horita, Z. In-situ production of bulk intermetallic-based nanocomposites and nanostructured intermetallics by high-pressure torsion. *Scr. Mater.* **2012**, *66*, 386–389.
201. Edalati, K.; Akiba, E.; Horita, Z. High-pressure torsion for new hydrogen storage materials. *Sci. Technol. Adv. Mater.* **2018**, *19*, 185–193. [CrossRef]
202. Révész, Á.; Gajdics, M. High-pressure torsion of non-equilibrium hydrogen storage materials: A review. *Energies* **2021**, *14*, 819. [CrossRef]
203. He, L.; Shi, X.; Li, X.; Huang, J.; Cheng, T.; Wang, X.; Li, Y.; Lin, H.; Edalati, K.; Li, H.W. Severe plastic deformation through high-pressure torsion for preparation of hydrogen storage materials—A review. *Mater. Trans.* **2023**, *64*, 1575–1584.
204. Edalati, K.; Akiba, E.; Botta, W.J.; Estrin, Y.; Floriano, R.; Fruchart, D.; Grosdidier, T.; Horita, Z.; Huot, J.; Li, H.W.; et al. Impact of severe plastic deformation on kinetics and thermodynamics of hydrogen storage in magnesium and its alloys. *J. Mater. Sci. Technol.* **2023**, *146*, 221–239. [CrossRef]
205. Reilly, J.J.; Wiswall, R.H. Formation and properties of iron titanium hydride. *Inorg. Chem.* **1974**, *13*, 218–222. [CrossRef]
206. Schlapbach, L.; Seiller, A.; Stucki, Y. Surface segregation in FeTi and its catalytic effect on the hydrogenation II: AES and XPS studies. *Mater. Res. Bull.* **1978**, *13*, 1031–1037. [CrossRef]
207. Yu, X.B.; Wu, Z.; Xia, B.J.; Xu, N.X. The activation mechanism of Ti-V-based hydrogen storage alloys. *J. Alloys Compd.* **2004**, *375*, 221–223.
208. Gross, K.J.; Chartouni, D.; Leroy, E.; Züttel, A.; Schlapbach, L. Mechanically milled Mg composites for hydrogen storage: The relationship between morphology and kinetics. *J. Alloys Compd.* **1998**, *269*, 259–270.

209. Dangwal, S.; Edalati, K. High-entropy alloy $TiV_2ZrCrMnFeNi$ for hydrogen storage at room temperature with full reversibility and good activation. *Scr. Mater.* **2024**, *238*, 115774.
210. Kawasaki, M.; Ahn, B.; Langdon, T.G. Microstructural evolution in a two-phase alloy processed by high-pressure torsion. *Acta Mater.* **2010**, *58*, 919–930. [CrossRef]
211. Sauvage, X.; Enikeev, N.; Valiev, R.; Nasedkina, Y.; Murashkin, M. Atomic scale analysis of the segregation and precipitation mechanisms in a severely deformed Al-Mg alloy. *Acta Mater.* **2014**, *72*, 125–136.
212. Wang, H.; Li, J.; Wei, X.; Zheng, Y.; Yang, S.; Lu, Y.; Ding, Z.; Luo, Q.; Li, Q.; Pan, F. Regulation for Mg-based hydrogen storage materials: Challenges, strategies, and perspectives. *Adv. Funct. Mater.* **2024**, *34*, 2406639. [CrossRef]
213. Khan, D.; Ong, W.J. Tailoring hydrogen storage materials kinetics and thermodynamics through nanostructuring, and nanoconfinement with in-situ catalysis. *Interdiscip. Mater.* **2025**, *4*, 249–283.
214. Gong, P.; Turk, A.; Nutter, J.; Yu, F.; Wynne, B.; Rivera-Diaz-del-Castillo, P.; Rainforth, W.M. Hydrogen embrittlement mechanisms in advanced high strength steel. *Acta Mater.* **2022**, *223*, 117488. [CrossRef]
215. Meda, U.S.; Bhat, N.; Pandey, A.; Subramanya, K.N.; Antony Raj, M.A.L. Challenges associated with hydrogen storage systems due to the hydrogen embrittlement of high strength steels. *Int. J. Hydrogen Energy* **2023**, *48*, 17894–17913. [CrossRef]
216. Todaka, Y.; Morisako, K.; Kumagai, M.; Matsumoto, Y.; Umemoto, M. Hydrogen embrittlement of submicrocrystalline ultra-low carbon steel produced by high-pressure torsion straining. *Adv. Mater. Res.* **2010**, *89–91*, 763–768.
217. Mine, Y.; Matsumoto, S.; Horita, Z. Strengthening and hydrogen embrittlement of ultrafine-grained Fe–0.01mass% C alloy processed by high-pressure torsion. *Corros. Sci.* **2011**, *53*, 2969–2977. [CrossRef]
218. Mine, Y.; Tachibana, K.; Horita, Z. Effect of high-pressure torsion processing and annealing on hydrogen embrittlement of type 304 metastable austenitic stainless steel. *Metall. Mater. Trans. A* **2010**, *41*, 3110–3120. [CrossRef]
219. Mine, Y.; Haraguchi, D.; Ideguchi, T.; Horita, N.; Horita, Z.; Takashima, K. Hydrogen embrittlement of ultrafine-grained austenitic stainless steels processed by high-pressure torsion at moderate temperature. *ISIJ Int.* **2016**, *56*, 1083–1090.
220. Mine, Y.; Koga, K.; Takashima, K.; Horita, Z. Mechanical characterisation of microstructural evolution in 304 stainless steel subjected to high-pressure torsion with and without hydrogen pre-charging. *Mater. Sci. Eng. A* **2016**, *661*, 87–95. [CrossRef]
221. Mohammadi, A.; Novelli, M.; Arita, M.; Bae, J.W.; Kim, H.S.; Grosdidier, T.; Edalati, K. Gradient-structured high-entropy alloy with improved combination of strength and hydrogen embrittlement resistance. *Corros. Sci.* **2022**, *200*, 110253. [CrossRef]
222. Mohammadi, A.; Edalati, P.; Arita, M.; Bae, J.W.; Kim, H.S.; Edalati, K. High strength and high ductility of a severely deformed high-entropy alloy in the presence of hydrogen. *Corros. Sci.* **2023**, *216*, 111097. [CrossRef]
223. Hongo, T.; Edalati, K.; Iwaoka, H.; Arita, M.; Matsuda, J.; Akiba, E.; Horita, Z. High-pressure torsion of palladium: Hydrogen-induced softening and plasticity in ultrafine grains and hydrogen-induced hardening and embrittlement in coarse grains. *Mater. Sci. Eng. A* **2014**, *618*, 1–8. [CrossRef]
224. Zhao, Y.; Lee, D.H.; Seok, M.Y.; Lee, J.; Phaniraj, M.P.; Suh, J.Y.; Ha, H.Y.; Kim, J.Y.; Ramamurty, U.; Jang, J. Resistance of CoCrFeMnNi high-entropy alloy to gaseous hydrogen embrittlement. *Scr. Mater.* **2017**, *135*, 54–58. [CrossRef]
225. Koyama, M.; Akiyama, E.; Lee, Y.K.; Raabe, D.; Tsuzaki, K. Overview of hydrogen embrittlement in high-Mn steels. *Int. J. Hydrogen Energy* **2017**, *42*, 12706–12723. [CrossRef]
226. Luo, H.; Lu, W.J.; Fang, X.F.; Ponge, D.; Li, Z.M.; Raabe, D. Beating hydrogen with its own weapon: Nano-twin gradients enhance embrittlement resistance of a high-entropy alloy. *Mater. Today* **2018**, *21*, 1003–1009.
227. Kim, D.H.; Moallemi, M.; Kim, K.S.; Cho, H.J.; Kim, S.J. Correlation between grain size variation and hydrogen embrittlement in a cost-effective $Fe_{40}Mn_{40}Ni_{10}Cr_{10}$ austenitic medium entropy alloy. *Int. J. Hydrogen Energy* **2023**, *48*, 5708–5717.
228. Bai, Y.; Momotani, Y.; Chen, M.C.; Shibata, A.; Tsuji, N. Effect of grain refinement on hydrogen embrittlement behaviors of high-Mn TWIP steel. *Mater. Sci. Eng. A* **2016**, *651*, 935–944. [CrossRef]
229. Momotani, Y.; Shibata, A.; Yonemura, T.; Bai, Y.; Tsuji, N. Effect of initial dislocation density on hydrogen accumulation behavior in martensitic steel. *Scr. Mater.* **2020**, *178*, 318–323. [CrossRef]
230. Faraji, G.; Torabzadeh, H. An overview on the continuous severe plastic deformation methods. *Mater. Trans.* **2019**, *60*, 1316–1330. [CrossRef]
231. Ivanisenko, Y. Perspectives of scaling up of severe plastic deformation: A case of high pressure torsion extrusion. *Mater. Trans.* **2023**, *64*, 1489–1496. [CrossRef]
232. Lowe, T.C.; Valiev, R.Z.; Li, X.; Ewing, B.R. Commercialization of bulk nanostructured metals and alloys. *MRS Bull.* **2021**, *46*, 265–272. [CrossRef]
233. Ghalehbandi, S.M.; Malaki, M.; Gupta, M. Accumulative roll bonding—A review. *Appl. Sci.* **2019**, *9*, 3627. [CrossRef]
234. Danaie, M.; Mauer, C.; Mitlin, D.; Huot, J. Hydrogen storage in bulk Mg–Ti and Mg–stainless steel multilayer composites synthesized via accumulative roll-bonding (ARB). *Int. J. Hydrogen Energy* **2011**, *39*, 3022–3036. [CrossRef]
235. Segal, V.M.; Reznikov, V.I.; Kopylov, V.I.; Pavlik, D.A.; Malyshev, V.F. *Processes of Plastic Structure Formation in Metals*; Nauka I Tehnika: Minsk, Belarus, 1994.

236. Raab, G.J.; Valiev, R.Z.; Lowe, T.C.; Zhu, Y.T. Continuous processing of ultrafine grained Al by ECAP–conform. *Mater. Sci. Eng. A* **2004**, *382*, 30–34. [CrossRef]
237. Beygelzimer, Y.; Estrin, Y.; Kulagin, R. Some unresolved problems of high-pressure torsion. *Mater. Trans.* **2023**, *64*, 1856–1865. [CrossRef]
238. Kulagin, R.; Beygelzimer, Y.; Estrin, Y.; Ivanisenko, Y.; Baretzky, B.; Hahn, H. A mathematical model of deformation under high pressure torsion extrusion. *Metals* **2019**, *9*, 306. [CrossRef]
239. Hohenwarter, A.; Pippan, R. Sample size and strain-rate-sensitivity effects on the homogeneity of high-pressure torsion deformed disks. *Metall. Mater. Trans. A* **2019**, *50*, 601–608. [CrossRef]
240. Sakai, G.; Nakamura, K.; Horita, Z.; Langdon, T.G. Developing high-pressure torsion for use with bulk samples. *Mater. Sci. Eng. A* **2005**, *406*, 268–273. [CrossRef]
241. Hohenwarter, A. Incremental high pressure torsion as a novel severe plastic deformation process: Processing features and application to copper. *Mater. Sci. Eng. A* **2015**, *626*, 80–85. [CrossRef]
242. Hohenwarter, A.; Pippan, R. Introduction of planar high pressure torsion (P-HPT) for fabrication of nanostructured sheets. *Adv. Eng. Mater.* **2018**, *20*, 1800050. [CrossRef]
243. Omranpour Shahreza, B.; Ivanisenko, J.; Sergejev, F.; Omranpour, H.; Huot, J. A novel approach in mechanical nanostructuring synthesis of metal hydride: Hydrogen sorption enhancement by high pressure torsion extrusion. *Int. J. Hydrogen Energy* **2024**, *51*, 133–142.
244. Toth, L.S.; Chen, C.; Pougis, A.; Arzaghi, M.; Fundenberger, J.-J.; Massion, R.; Suwas, S. High pressure tube twisting for producing ultra fine grained materials: A review. *Mater. Trans.* **2019**, *60*, 1177–1191. [CrossRef]
245. Li, Z.; Liu, Y.; Wang, J.T.; Langdon, T.G. Tube high-pressure shearing: A simple shear path to unusual microstructures and unprecedented properties. *Mater. Trans.* **2023**, *64*, 1449–1463. [CrossRef]
246. Popova, E.N.; Popov, V.V.; Romanov, E.P.; Pilyugin, V.P. Thermal stability of nanocrystalline Nb produced by severe plastic deformation. *Phys. Met. Metallogr.* **2006**, *101*, 52–57.
247. Popov, V.V.; Popova, E.N. Behavior of Nb and Cu-Nb composites under severe plastic deformation and annealing. *Mater. Trans.* **2019**, *60*, 1209–1220.
248. Huang, Y.; Sabbaghianrad, S.; Almazrouee, A.I.; Al-Fadhalah, K.J.; Alhajeri, S.N.; Langdon, T.G. The significance of self-annealing at room temperature in high purity copper processed by high-pressure torsion. *Mater. Sci. Eng. A* **2016**, *656*, 55–66.
249. Wang, C.T.; He, Y.; Langdon, T.G. The significance of strain weakening and self-annealing in a superplastic Bi–Sn eutectic alloy processed by high-pressure torsion. *Acta Mater.* **2020**, *185*, 245–256.
250. Horita, Z.; Tang, Y.; Matsuo, M.; Edalati, K.; Yumoto, M.; Takizawa, Y. Enhancement of activation and hydrogen storage kinetics of TiFe(Mn) using high-pressure sliding (HPS) process. *Mater. Trans.* **2023**, *64*, 1920–1923. [CrossRef]
251. Keil, T.; Taheriniya, S.; Bruder, E.; Wilde, G.; Durst, K. Effects of solutes on thermal stability, microstructure and mechanical properties in CrMnFeCoNi based alloys after high pressure torsion. *Acta Mater.* **2022**, *227*, 117689.
252. Bazarnik, P.; Emerla, M.; Huang, Y.; Wojciechowska, A.; Ciemiorek, M.; Bednarczyk, W.; Jastrzębska, A.; Lewandowska, M.; Langdon, T.G. Enhanced thermal stability of nanocrystalline Cu composites processed by high-pressure torsion: The pinning effect of Al_2O_3, GO, and rGO/Al_2O_3 nanoparticles. *J. Alloys Compd.* **2025**, *1033*, 181283.
253. Krystian, M.; Zehetbauer, M.J.; Kropik, H.; Mingler, B.; Krexner, G. Hydrogen storage properties of bulk nanostructured ZK_{60} Mg alloy processed by equal channel angular pressing. *J. Alloys Compd.* **2011**, *509*, S449–S455. [CrossRef]
254. Cengeri, P.; Kimoto, Y.; Janoska, M.; Abbasi, Z.; Morisada, Y.; Fujii, H.; Enzinger, N.; Sommitsch, C.; Boczkal, G.; Krexner, G.; et al. Long term hydrogen storage properties of ZK_{60} Mg-alloy as processed by different methods of SPD. *J. Mater. Sci.* **2024**, *59*, 5906–5922. [CrossRef]
255. Asgharzadeh, H.; Joo, S.H.; Lee, J.K.; Kim, H.S. Consolidation of Cu-based amorphous alloy powders by high-pressure torsion. *J. Mater. Sci.* **2015**, *50*, 3164–3174. [CrossRef]
256. Castro, M.M.; Pereira, P.H.R.; Isaac, A.; Langdon, T.G.; Figueiredo, R.B. Inverse Hall–Petch behaviour in an AZ91 alloy and in an AZ91–Al_2O_3 composite consolidated by high-pressure torsion. *Adv. Eng. Mater.* **2020**, *22*, 1900894.
257. Cheng, H.; Wang, J.; Zhao, Y.; Han, X. Effect of phase composition, morphology, and specific surface area on the photocatalytic activity of TiO_2 nanomaterials. *RSC Adv.* **2014**, *4*, 47031–47038. [CrossRef]
258. Chen, D.; Ai, S.; Liang, Z.; Wei, F. Preparation and photocatalytic properties of zinc oxide nanoparticles by microwave-assisted ball milling. *Ceram. Int.* **2016**, *42*, 3692–3696. [CrossRef]
259. Dzik, P.; Svoboda, T.; Kaštyl, J.; Veselý, M. Modification of photocatalyst morphology by ball milling and its impact on the physicochemical properties of wet coated layers. *Catal. Today* **2019**, *328*, 65–70. [CrossRef]
260. Wang, H.; Li, G.; Jia, L.; Wang, G.; Tang, C. Controllable preferential-etching synthesis and photocatalytic activity of porous ZnO nanotubes. *J. Phys. Chem. C* **2008**, *112*, 11738–11743.

261. Zhang, P.; Huang, Y.; Rao, Y.; Chen, M.; Li, X.; Ho, W.; Lee, S.; Cao, J. Chemical etching fabrication of uniform mesoporous Bi@Bi_2O_3 nanospheres with enhanced visible light-induced photocatalytic oxidation performance for NO_x. *Chem. Eng. J.* **2021**, *406*, 126910. [CrossRef]
262. Gubicza, J. Lattice defects and their influence on the mechanical properties of bulk materials processed by severe plastic deformation. *Mater. Trans.* **2019**, *60*, 1230–1242. [CrossRef]
263. Wilde, G.; Divinski, S. Grain boundaries and diffusion phenomena in severely deformed materials. *Mater. Trans.* **2019**, *60*, 1302–1315. [CrossRef]
264. Ren, P.; Song, M.; Lee, J.; Zheng, J.; Lu, Z.; Engelhard, M.; Yang, X.; Li, X.; Kisailus, D.; Li, D. Edge dislocations induce improved photocatalytic efficiency of colored TiO_2. *Adv. Mater. Interfaces* **2019**, *6*, 1901121. [CrossRef]
265. Wang, B.; Liu, J.; Yao, S.; Liu, F.; Li, Y.; He, J.; Lin, Z.; Huang, F.; Liu, C.; Wang, M. Vacancy engineering in nanostructured semiconductors for enhancing photocatalysis. *J. Mater. Chem. A* **2021**, *9*, 17143–17172. [CrossRef]
266. Kamei, M. Localization of the photocatalytic reaction on the grain boundary of bicrystalline TiO_2. *Appl. Phys. Express* **2008**, *1*, 101201. [CrossRef]
267. Wei, Y.; Zhou, Z.; Fang, W.-H.; Long, R. Grain boundary facilitates photocatalytic reaction in rutile TiO_2 despite fast charge recombination: A time-domain ab initio analysis. *J. Phys. Chem. Lett.* **2018**, *9*, 5884–5889. [CrossRef]
268. Alawadhi, M.Y.; Aloraier, A.S.; Alaskari, A.M.; Alazemi, A.A.; Huang, Y. Effects of short-term annealing on the thermal stability and microstructural evolution of oxygen-free copper processed by high-pressure torsion. *Materials* **2024**, *17*, 5886. [PubMed]
269. Dai, Y.; Ahmadian, A.; Petry, O.; Sos, M.; Schwotzer, M.; Durst, K.; Kübel, C. Microstructural evolution and mechanical properties of $CuSn_5$ processed by HPT followed by short-time annealing. *Mater. Des.* **2025**, *259*, 114897.

Disclaimer/Publisher's Note: The statements, opinions and data contained in all publications are solely those of the individual author(s) and contributor(s) and not of MDPI and/or the editor(s). MDPI and/or the editor(s) disclaim responsibility for any injury to people or property resulting from any ideas, methods, instructions or products referred to in the content.